

ABSTRACT

JIANG, HAN. Centrifugally-spun Nanofibers and Their Energy Storage Applications. (Under the direction of Dr. Xiangwu Zhang).

Electrospinning is currently the dominating method to produce carbon nanofibers. However, it is bottlenecked by various drawbacks: (1) low production rate, (2) complexity of device scale-up, and (3) relatively high production cost. Centrifugal spinning, on the other hand, is featured by its several magnitudes higher production rate, without the application of high voltage and ease of scaling-up.

Carbon nanofiber (CNF), a typical one-dimensional nanomaterial, is featured by its high specific area, high aspect ratio, good conductivity and mechanical properties. Typical applications of CNFs can be found in areas such as energy storage, sensor, catalyst and biological scaffold. The combination of electrospun CNFs with active materials yields a promising category of composite material and such composite can be used as energy storage material in lithium-ion batteries or supercapacitors. Lithium-ion batteries have high energy density while supercapacitors are featured by high power density. These two systems often cooperate with each other, offering high power and energy densities required by the ever increasing demand of portable electronics, electric vehicles and hybrid electric vehicles.

CNF-based materials prepared from electrospinning have been widely studied as electrodes for lithium-ion batteries and supercapacitors. However, the low production rate of electrospinning greatly hinders the large-scale production of CNF-based materials. In our work, CNF-based materials were prepared by centrifugal spinning combined with subsequent heat treatment and were used as electrode materials for both lithium-ion batteries and

supercapacitors. The electrochemical performance of CNF-based materials demonstrates that centrifugal spinning is a promising alternative to fabricate nanofibers for energy storage applications.

© Copyright 2014 Han Jiang

All Rights Reserved

Centrifugally-Spun Nanofibers and Their Energy Storage Applications

by
Han Jiang

A thesis submitted to the Graduate Faculty of
North Carolina State University
in partial fulfillment of the
requirements for the degree of
Master of Science

Textile Chemistry

Raleigh, North Carolina

2014

APPROVED BY:

Dr. Xiangwu Zhang
Committee Chair

Dr. Stephen Michielsen

Dr. Philip Bradford

Dr. Richard Kotek

DEDICATION

*To my loving parents and family members,
without whose patience, support, guidance and love,
all these would be impossible to achieve.*

*I am a caterpillar in the tree,
you teach me happiness and to think,
flying away I will be,
you just smile and believe.*

BIOGRAPHY

Han Jiang was born on September 22nd, 1989 in Lishui, Zhejiang, P.R. China. He completed his high school education at Hangzhou High School Attached to Zhejiang University, and then went to northern China to pursue his undergraduate study at Shenyang Institute of Technology in September 2008. He graduated with a dual bachelor degree in the fields of polymer science and engineering and English literature in July 2012.

In August 2012, Han Jiang came to the U.S. and started pursuing his master degree majoring in Textile Chemistry in the Department of Textile Engineering, Chemistry and Science at North Carolina State University, Raleigh, North Carolina. His research activities range from fabrication and characterization of centrifugally-spun nanofibers, carbonaceous materials and their applications for energy conversion and storage systems. Besides research works, Han Jiang also enjoy travelling, learning history, listening to music, watching movies, playing games and reading.

ACKNOWLEDGMENTS

The author would like to offer his heartfelt appreciation to Dr. Xiangwu Zhang, for his great mentorship, encouragements, patience, helps and selfless sharing of knowledge during the author's growth in his master studies years. The author's work and this very thesis cannot be finished without his guidance and thanks to Dr. Zhang, the research work became so much more interesting and rewarding to the author. Thanks also go to his other committee members: Dr. Stephen Michielsen, Dr. Philip Bradford and Dr. Richard Kotek, who have lectured and enlightened the author for their informative teachings. Their wise counsel, advice, and support will always be with the author.

The author would also like to thank his research group members: Dr. Shu Zhang, Dr. Leigang Xue, Dr. Shuli Li, Dr. Ying Li, Mr. Kun Fu, Mr. Guanjie Xu, Mr. Yao Lu, Mr. Chen Chen, Mr. Jiadeng Zhu, Mr. Liangqu Chen, Mr. Mahmut Dirican, Ms. Meltem Yanilmaz, Ms. Xin Xia, Ms. Ying Ji, Dr. Hongbin Tan and Ms. Yeqian Ge at North Carolina State University for their warmhearted helps and encouragements during his master study years. The author also deeply appreciates Mr. Chuck Mooney from Analytical Instrumentation Facility, Dr. Dhana Savithri from IBRI Analytical Service Center, Mr. Chris Pernell from the Department of Food, Bioprocessing and Nutrition Sciences, Ms. Birgit Anderson and Ms. Judy Elson from the College of Textiles for their kindly helps in sample characterizations.

TABLE OF CONTENTS

LIST OF TABLES	viii
LIST OF FIGURES	ix
CHAPTER 1 INTRODUCTION	1
1.1 Nanofibers.....	1
1.2. Formation of nanofibers.....	2
1.2.1 Electrospinning	3
1.2.1.1 Related work	5
1.2.2 Multi-component fiber spinning	9
1.2.3 Centrifugal spinning.....	11
1.3. Carbon nanofiber based materials for lithium-ion-batteries	20
1.3.1 Working principle	21
1.3.2 Recent advances in anode materials.....	23
1.3.2.1 Graphenes	23
1.3.2.2 Graphites.....	24
1.3.2.3 Carbon nanotubes.....	25
1.3.2.4 Carbon nanofibers.....	27
1.3.3 Carbon group alloying elements and composites.....	30
1.4. Supercapacitors	37
1.4.1 Working principle	38
1.4.2 Impacting factors and electrode materials	40
CHAPTER 2 OBJECTIVES.....	44

CHAPTER 3 CENTRIFUGALLY-SPUN TIN-CONTAINING CARBON NANOFIBERS AS ANODE MATERIAL FOR LITHIUM-ION BATTERIES	52
3.1. Introduction.....	53
3.2. Experimental.....	55
3.2.1 Materials	55
3.2.2. Centrifugal spinning and thermal treatment	55
3.2.3 Structure characterization and electrochemical evaluation.....	55
3.3. Results and discussion	57
3.3.1 Solution properties.....	57
3.3.2 Composition and morphology.....	62
3.3.3 Electrochemical performance	65
3.4. Conclusion	69
CHAPTER 4 POROUS CARBON NANOFIBERS PREPARED BY CENTRIFUGAL SPINNING AS ELECTRODE MATERIAL FOR SUPERCAPACITORS.....	70
4.1. Introduction.....	71
4.2. Experimental.....	73
4.2.1 Materials and preparation of carbon nanofibers	73
4.2.2 Solution property and fiber structure characterizations	74
4.2.3 Electrochemical measurements.....	75
4.3. Results and discussion	75
4.3.1 Structure Characterization	75
4.3.2 Electrochemical characterization	81

4.4. Conclusion	84
CHAPTER 5 CONCLUSIONS	86
CHAPTER 6 RECOMMENDATION WORK.....	88
6.1. High speed camera observation upon fiber formation process during centrifugal spinning.....	88
6.2. Centrifugally-spun core-shell silicon-enwrapped nanofibers for use as anode in lithium-ion batteries.....	88
6.3. Centrifugally-spun nanofibers for use as electrode for pseudocapacitors.	89
REFERENCES	90

LIST OF TABLES

Table 3.1 Effects of PAN and SnCl ₂ on the -C=O and OC-N stretching peaks of DMF. .59	
Table 3.2 Compositions of Sn/C nanofibers prepared by centrifugal spinning.62	
Table 4.1 Physicochemical characterizations of CNFs thermally-treated from PAN/PMMA precursors with different weight ratios at 800 °C.80	

LIST OF FIGURES

Figure 1.1. Illustration of nanofibers with multilevel micro-/nanostructures and their applications.	2
Figure 1.2. Publication numbers on the subject of electrospinning provided by the search engine Scopus (keyword: electrospinning).	3
Figure 1.3. Schematic representation of a typical laboratory type electrospinning setup. ..	4
Figure 1.4. Schematic of a rotating drum type electrospinning setup.	5
Figure 1.5. (A) Schematic of a spinneret containing two coaxial capillaries in a modified electrospinning setup. (B) TEM image of the as-spun hollow nanofibers with amorphous TiO ₂ / polyvinylpyrrolidone composite as the wall.	6
Figure 1.6. SEM image of a uniaxially aligned array of TiO ₂ hollow fibers.	7
Figure 1.7. SEM images of multichannel tubes with various numbers of channels: (a) two, (b) three, (c) four and (d) five. The inset in each figure shows the cross section illustration of the spinneret used to fabricate the tube. Scale bars are 100 nm.	8
Figure 1.8. (Left) Cross-sectional SEM image of the TiO ₂ fibers, showing the nanowire-in-nanotube structure. (Right) TEM image of a single fiber showing a continuous nanowire in the microtube.	8
Figure 1.9. Schematic of islands-in-the-sea fiber fabrication by melt blowing.	10
Figure 1.10. Schematic of an islands-in-the-sea bi-component fiber, where PAN/CNT is the island and PMMA is the sea.	11
Figure 1.11. SEM of bi-component fibers. (a) Low magnification image showing the separation of island fibers (PAN/CNT) from the islands-in-a-sea structure while removing	

the sea component (PMMA), and (b) high magnification image of circled region from left image showing the separation of individual islands fiber.....11

Figure 1.12. Schematic diagram showing a laboratory setup for centrifugal spinning.13

Figure 1.13. Schematic of nanofiber formation during centrifugal spinning: (i) jet-initiation, (ii) jet-extension, (iii) solvent-evaporation.....13

Figure 1.14. SEM images of 12wt% CNT/PMMA composite nanofibers.18

Figure 1.15. Tensile strength-strain curves of CNT/PMMA nanofibers with different CNT contents: (1) 0wt%, (2) 3wt%, (3) 8wt%, and (4) 12wt%.19

Figure 1.16. (A) Cyclic voltammetry curves, and (B) cycling performance of the vanadium oxide-filled carbon nanofibers. Inset in B shows the charge/discharge curves for the 2nd, 5th and 30th cycles.20

Figure 1.17. Comparison of the different battery technologies in terms of volumetric and gravimetric energy densities.21

Figure 1.18. A lithium ion cell based on lithium-metal oxide cathode and graphite anode.22

Figure 1.19. Schematic of lithium intercalation in graphite: (A) lithium is inserted in every second carbon hexagon and (B) between the graphite layers.25

Figure 1.20. Charge-discharge curves (a), rate performance (b), cycling performance (c), and coulombic efficiency (d) of CNT anodes.....26

Figure 1.21. Mechanisms of the stabilization and subsequent carbonization of PAN.29

Figure 1.22. Schematic of Si–C composite assembly. a–c, Annealed carbon-black dendritic particles (a) are coated by Si nanoparticles (b) and then assembled into rigid spheres with open interconnected internal channels during C deposition (c).....31

Figure 1.23. SEM images of the silicon/CNF composite: uniformly distributed nanosized Si nodules on the exterior and interior surface of CNFs.....31

Figure 1.24. Schematic illustration of the reversible structural changes of the coaxially coated Si on vertically aligned CNFs in (a) extracted (discharged) and (b) inserted (charged) states.32

Figure 1.25. Cycling performance of a 10 mm long vertically aligned CNF array coated with 0.5 μm Si.....32

Figure 1.26. Schematic for preparing porous multichannel carbon microtubes containing Sn nanoparticles.33

Figure 1.27. Cycling performance of Sn encapsulated in porous multichannel carbon microtubes (SPMCT) and commercial Sn; the inset displays the discharge capacities of SPMCT electrodes at 2 and 10 C.....34

Figure 1.28. (Left) Charge-discharge performance (Right) cycling performance of Sn/C non-woven films.35

Figure 1.29. TEM images (a,b), microstructures (c), and HRTEM image (d) of the tin/tin oxides encapsulating porous carbon nanofibers.36

Figure 1.30. Charge/discharge profiles (left) and cycling performance (right) of the tin/tin oxides encapsulating porous carbon nanofibers.36

Figure 1. 31. Comparing power sources: energy versus power densities (Ragone plot).....	38
Figure 1.32. Schematic illustration of an electric double layer capacitor.....	39
Figure 1.33. Schematic of the ion size and pore size effect on nanoporous carbon electrode.....	41
Figure 1.34. The dependence of specific capacitance on pore diameter and BET surface area.....	42
Figure 1.35. The dependence of specific capacitance on micro- and mesopore volumes.	42
Figure 1.36. CV curves of the 900 °C and 1000 °C carbonized/activated samples at a scan rate of 2 mV/s in (a) 1 mol L ⁻¹ H ₂ SO ₄ and (b) 6 mol L ⁻¹ KOH.	43
Figure 3.1. a) Schematic of centrifugal spinning machine setup, and b) the real-time photo of centrifugal spinning process.	54
Figure 3.2. FTIR spectra of PAN/DMF with different SnCl ₂ concentrations: (a) DMF, (b) 0, (c) 2 wt%, (d) 5 wt%, (e) 8 wt%.	58
Figure 3.3. Depiction of the molecular structures and interactions among PAN, DMF and SnCl ₂	59
Figure 3.4. Specific viscosity versus Sn salt concentration profile for PAN/DMF solutions.	60
Figure 3.5. Surface tension versus Sn salt concentration profile for PAN/DMF solutions.	61
Figure 3.6. SEM images of tin salt/PAN precursor fibers with different weight ratios of PAN/SnCl ₂ : a)15/0, b) 15/2, c) 15/5, d) 15/8.....	63

Figure 3.7. SEM images of Sn/C composite nanofibers derived from different weight ratios of PAN/SnCl ₂ precursors: a,b) 15/2, c,d) 15/5, e,f) 15/8.	64
Figure 3.8. TEM image of a Sn/C composite nanofiber derived from 5 wt% SnCl ₂ /PAN precursor.	65
Figure 3.9. Galvanostatic Charge-discharge curves of Sn/C nanofiber anodes derived from: (a) 0 wt%, (b) 2 wt%, (c) 5 wt% and (d) 8wt% SnCl ₂ /PAN precursors.	67
Figure 3.10. Cycling performance of Sn/C nanofiber anodes derived from 0, 2, 5 and 8 wt% SnCl ₂ /15wt% PAN precursors.	68
Figure 4.1. Schematic of the preparation of porous carbon nanofibers by centrifugal spinning of PAN/PMMA blend.	73
Figure 4.2. Specific viscosity versus PAN/PMMA weight ratios.	76
Figure 4.3. Centrifugally-spun PAN/PMMA nanofibers with different PAN/PMMA weight ratios: a) 1:9, b) 2:8, c) 3:7, d) 5:5.	77
Figure 4.4. SEM images of carbon nanofibers thermally-treated from centrifugally-spun PAN/PMMA precursors with different weight ratios: (a,b) 1:9, (c,d) 2:8, (e,f) 3:7, (g,h) 5:5.	79
Figure 4.5. CV curves of carbon nanofibers with 3:7 PAN/PMMA weight ratio, and thermally-treated at: (a) 700 °C and (b) 800 °C. Arrows indicate the increasing scan rate from 10 to 100 mV s ⁻¹	82
Figure 4.6. Nyquist plots for carbon nanofibers prepared from PAN/PMMA precursor fibers with a weight ratio of 3:7 at 700 °C, 800 °C. The impedance was tested at an open circuit voltage of 5 mV.	84

CHAPTER 1 INTRODUCTION

1.1 Nanofibers

Nanofibers, a crucial one-dimensional nanostructure, have attracted much attention due to their unique properties and intriguing applications in many areas. Nanofibers acquire cylindrical or conical contours with diameters usually less than 1000 nm while the internal structure of carbon nanofibers varies and is comprised of different arrangements of modified graphene sheets. It is electronically conductive,[1] which can lead to electrochemical applications. Tailored carbon nanofibers can serve as matrix material for energy storage composite materials, with their excellent mechanical and chemical stability, carbon nanofibers can not only contribute to the power output, but also help to enhance cycling performance and energy density.[2]

Currently, methods to fabricate nanofibers include but are not limited to bi-component fiber spinning [3], phase separation [4], and template synthesis [5]. The resultant nanofibers can be applied in filtration [6], tissue engineering [7], drug delivery [8], sensor [9], catalysis [10], energy storage [11-16], etc. Figure 1.1 shows various applications of nanofibers with different multilevel micro-/nano structures.

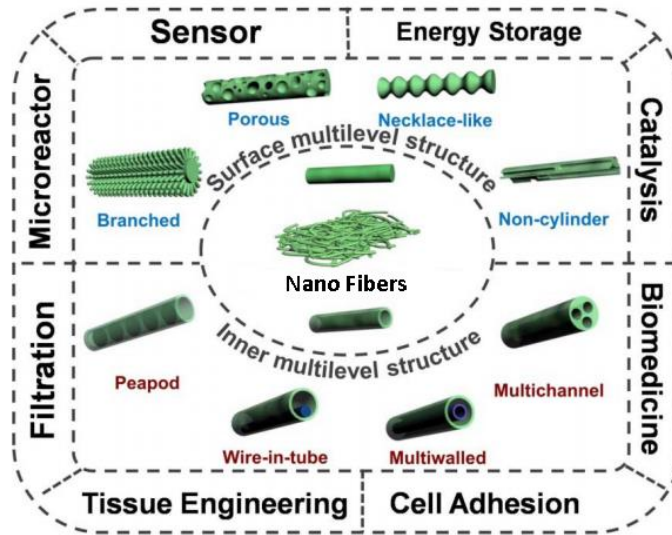


Figure 1.1. Illustration of nanofibers with multilevel micro-/nanostructures and their applications.[17]

As mentioned above, nanofibers possess unique properties such as high surface-to-volume ratio, which helps increase interactions with targeted substrates and offers more anchor sites for active materials compared to other micro- to macro-size counterparts. Therefore, it is believed that nanofibers are a promising candidate as cutting-edge functional materials.

1.2 Formation of nanofibers

Among various nanofiber fabrication techniques, electrospinning is currently the most investigated nanofiber preparation method (Figure 1.2).[18] In the year of 2012 alone, there were over 1400 peer-reviewed journal publications on electrospinning, and more than half of the publications focused on the investigation of the electrospinning process and the

characterization analysis while the other half concentrated on the innovative applications of the resultant electrospun nanofibers.

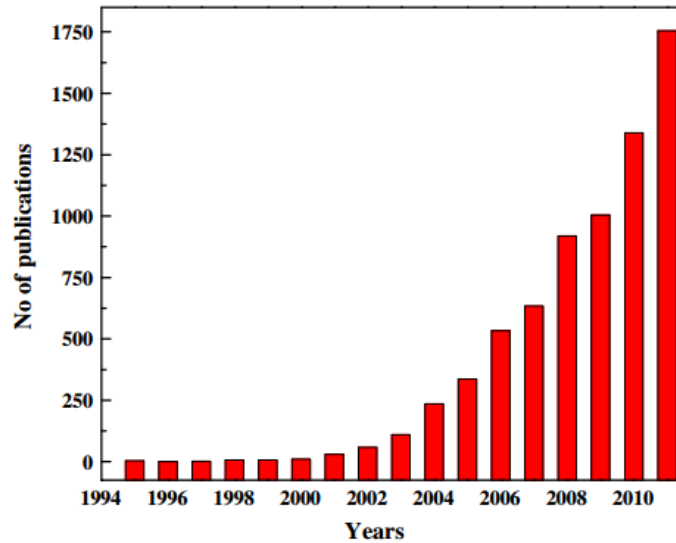


Figure 1.2. Publication numbers on the subject of electrospinning provided by the search engine Scopus (keyword: electrospinning).[18]

1.2.1 Electrospinning

The electrospinning method can be considered as a variant of electrospaying.[19] Early in 1934, Formals disclosed an apparatus, by utilizing accumulated surface charges on the spinning solution surface to fabricate polymer filaments.[20] In early 1990s, D.H. Reneker et al. explored the possibility of using electrospinning to fabricate various polymer thin fibers.[21] Since then, the word *electrospinning* was coined and widely used in the academia and industry, triggered abundant research interests.

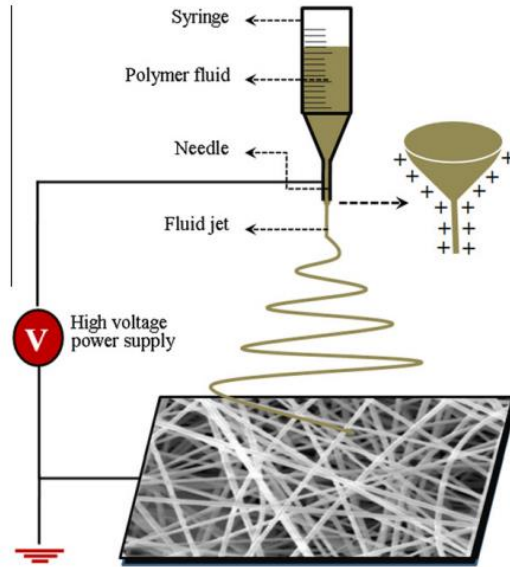


Figure 1.3. Schematic representation of a typical laboratory type electrospinning setup.[18]

A typical laboratory type electrospinning setup is shown in Figure 1.3. It mainly composes of three components: a high voltage power supply, a spinneret and a collector. Although the electrospinning setup looks quite simple, the actual mechanisms behind are complicated. Before 1999, the formation of fibers by electrospinning was often ascribed to the splitting or splaying of the electrified jet due to repulsion between surface charges.[21] Recently, researchers unveiled that the thinning of a jet during electrospinning is mainly caused by the bending instability associated with the electrified jet. D.H. Reneker et al. treated the charged liquid jet as “a system of connected, viscoelastic dumbbells”.[22]

Parameters such as solution concentration, viscosity, surface tension and net charge density of the polymer jet affect the morphology of the resultant fibers. For example, solution

concentration is considered as a major factor that affects the fiber diameter. In general, fiber diameter increases with increasing solution concentration. The morphology of fibers also has a strong dependence on solution viscosity and surface tension.[23, 24]

1.2.1.1 Related work

Modifications of the electrospinning setup have been proposed to enhance the applicability of electrospinning. For instance, relatively large areal nanofiber webs have been collected by introducing a rotating drum into the setup (Figure 1.4).[25, 26] Many other electrospinning systems have also been designed such as rotary cone combining with needleless spinneret. However, the complex system setup still remains as a headache for industrial scale-up.[27, 28]

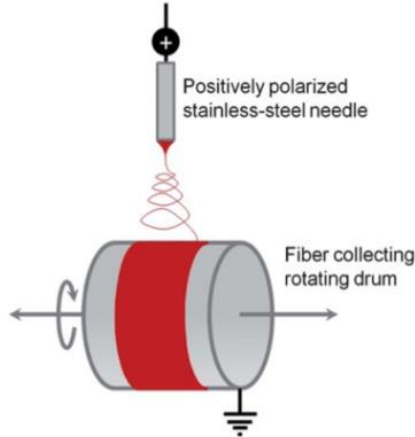


Figure 1.4. Schematic of a rotating drum type electrospinning setup.[29]

Various polymers such as polyacrylonitrile (PAN) [30], poly(methyl methacrylate) [31] and polystyrene [32] have been successfully electrospun into fine fibers. At the same time,

structural variations of nanofibers, including core-shell nanofibers [26], multilayered fibers [29], hollow fibers [33] (Figure 1.6) have been designed and fabricated by modified electrospinning and applied to different areas.

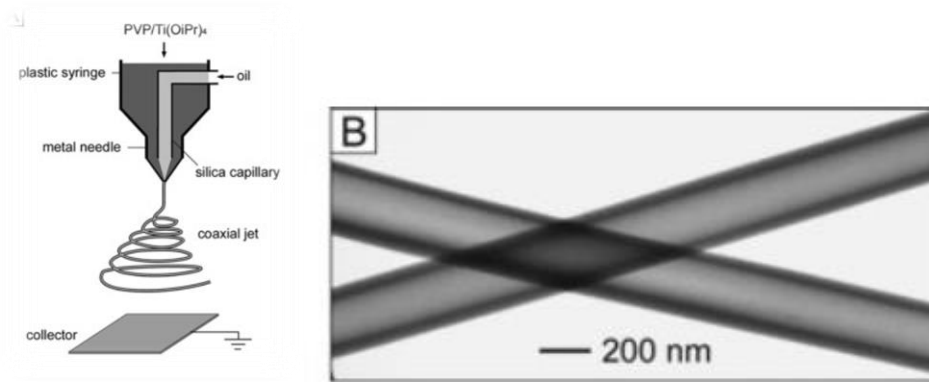


Figure 1.5. (A) Schematic of a spinneret containing two coaxial capillaries in a modified electrospinning setup. (B) TEM image of the as-spun hollow nanofibers with amorphous TiO₂/ polyvinylpyrrolidone composite as the wall.[26]

Recently, Xia et al. prepared hollow nanofibers by the electrospinning of two immiscible liquids through a coaxial, two-capillary spinneret, followed by selective removal of the cores.[33] Figure 1.5 (A) shows the setup for the modified electrospinning setup while Figure 1.5 (B) shows the TEM image of the resultant core-shell nanofibers. Dark walls and bright core were observed, indicating successful attempt to fabricate the core-shell structural nanofibers by electrospinning. Figure 1.6 shows the morphology of the anatase hollow fibers. By changing experiments parameters, the nanofiber size and wall thickness could be altered.

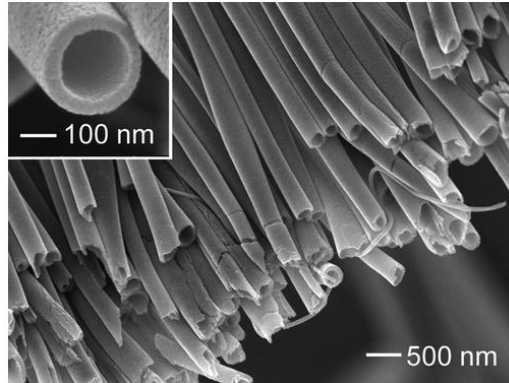


Figure 1.6. SEM image of a uniaxially aligned array of TiO_2 hollow fibers.[33]

Figure 1.7 shows the multichannel tube morphology prepared by Jiang and co-workers by utilizing multifluidic compound jet electrospinning technique.[34] An ethanol solution of $\text{Ti}(\text{OiPr})_4$ and poly(vinyl pyrrolidone) was used as outer liquid, while a commercially available innocuous paraffin oil was selected for inner liquid. Subsequent thermal treatment removed the paraffin oil, leading to the formation of multichannel hollow nanofibers.

A novel TiO_2 nanowire-in-microtube structure was recently reported by Jiang's group.[35] By adding a proper middle fluid as a protective fluid, which acts as spacer between the core fluid and shell fluid, even mutually miscible fluids can be made into core-shell nanofibers. Figure 1.8 shows the cross-sectional SEM and TEM images of the resultant nanowire-in-nanotube nanofibers.

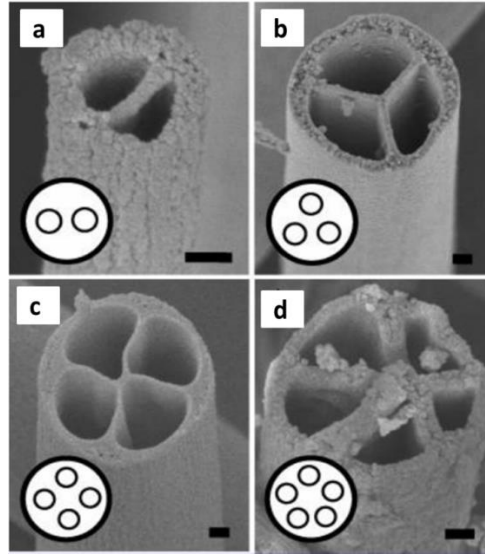


Figure 1.7. SEM images of multichannel tubes with various numbers of channels: (a) two, (b) three, (c) four and (d) five. The inset in each figure shows the cross section illustration of the spinneret used to fabricate the tube. Scale bars are 100 nm.[34]

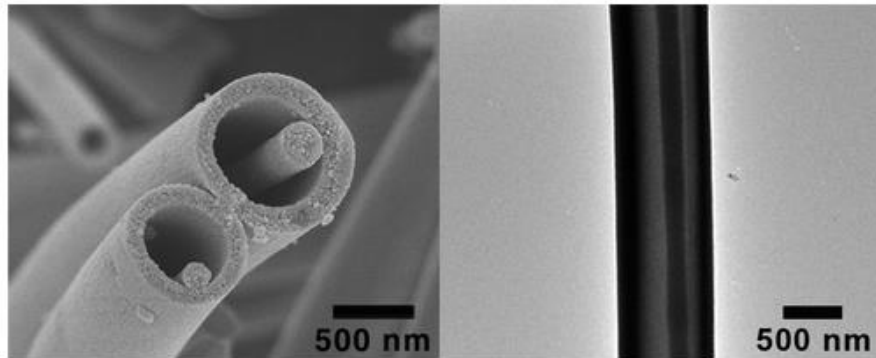


Figure 1.8. (Left) Cross-sectional SEM image of the TiO_2 fibers, showing the nanowire-in-nanotube structure. (Right) TEM image of a single fiber showing a continuous nanowire in the microtube.[34, 35]

Taking advantage of nanofibers' unique properties, applications such as filtration [36], adhesives [37] were extensively reported for electrospun nanofibers. By providing 3-D environment for cells and tissues to grow, electrospun fibers have also been applied to tissue engineering field.[38, 39] For instance, antibiotics, anticancer agents, proteins, DNA, and RNA can be incorporated into electrospun scaffolds.[40, 41] Protective textiles with better thermal insulation, chemical resistance can also be fabricated based upon electrospun nanofibers.[42, 43] By doping different kinds of additives into electrospun fibers, applications can also be found in ultrasensitive sensors for acoustic, resistive, photoelectric, optic resources.[9, 44, 45]

1.2.2 Multi-component fiber spinning

Spinning immiscible polymer blends offers a facile approach to generate fibers with diameters as small as tens of nanometers. F.S. Bates et al. reported the fabrication of island-in-the-sea polymer fibers by using melt-blowing method, followed by selectively removal of the majority phase (sea) with a solvent to form nanofibers.[3] Figure 1.9 shows the schematic of nanofiber formation by melt-blowing.

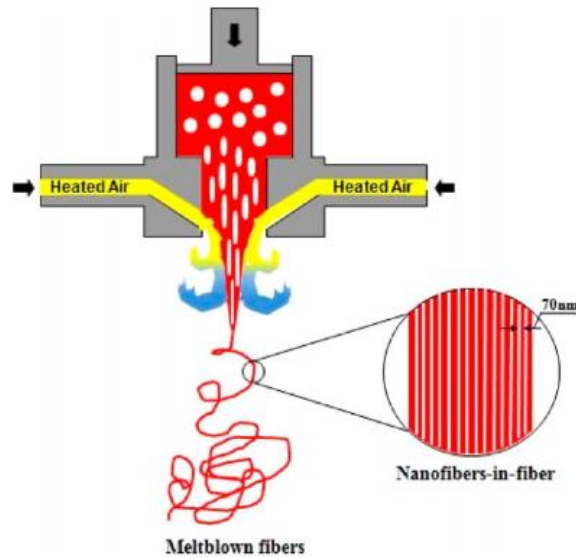


Figure 1.9. Schematic of islands-in-the-sea fiber fabrication by melt blowing.[3]

Kumar and co-workers reported CNT reinforced PAN nanofibers prepared by the removal of the sea component from the island-in-the-sea precursor nanofibers, where CNT-reinforced PAN is the island and poly methyl methacrylate (PMMA) is the sea.[46] Figures 1.10 and 1.11 show the schematic, formation and SEM images of the CNT-reinforced PAN nanofibers.

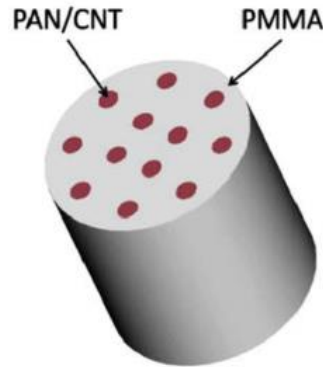


Figure 1.10. Schematic of an islands-in-the-sea bi-component fiber, where PAN/CNT is the island and PMMA is the sea.[46]

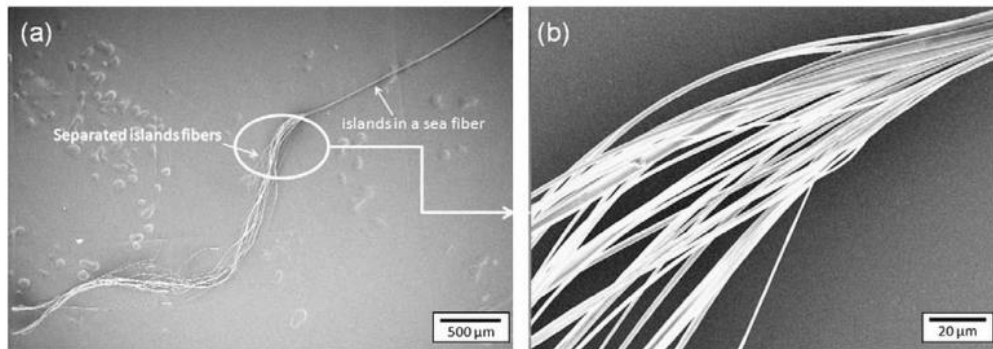


Figure 1.11. SEM of bi-component fibers. (a) Low magnification image showing the separation of island fibers (PAN/CNT) from the islands-in-a-sea structure while removing the sea component (PMMA), and (b) high magnification image of circled region from left image showing the separation of individual islands fiber.[46]

1.2.3 Centrifugal spinning

Centrifugal spinning, or ForcespinningTM, is a recently developed nanofiber forming technique and it draws extensive attention mainly due to its high production rate, which is 500 times faster than traditional electrospinning.[47] Instead of using electrostatic force, centrifugal spinning utilizes centrifugal force to realize the high-rate production of

nanofibers.[48] Centrifugal spinning can be used to produce nanofibers by using polymer solutions or polymer melts, without the dielectric constant limitations and the involvement of high voltage electric field. Besides, carbon, ceramic and metal fibers can also be fabricated by centrifugal spinning.[28]

1.2.3.1 Working principle

Figure 1.12 shows a schematic diagram of a laboratory centrifugal spinning device, which is mainly composed of a nozzle-contained spinneret, a high-speed motor, which is used to rotate the spinneret, a speed controller, which can adjust the rotational speed of the spinneret, flexible air foils, which are attached to the bottom of the spinneret to generate air turbulence and accelerate the solvent evaporation, and fiber collectors.

The fiber formation process of centrifugal spinning relies upon the competition between centrifugal force and Laplace force (arise from surface curvature).[49] During centrifugal spinning, the nanofiber formation process can be separated into three stages: (i) jet-initiation to induce flow of the polymer solution through the orifice, (ii) jet-extension to increase surface area of the propelled polymer stream, and (iii) solvent evaporation to solidify and shrink the polymer jet (Figure 1.13).[50] In general, as long as the centrifugal force is able to overcome the surface tension of the solution, liquid jet can be ejected from the spinneret orifice. The solution jet then undergoes a stretching process, accompanied by rapid solvent evaporation, and eventually nanofibers can be collected on the collectors.[51]

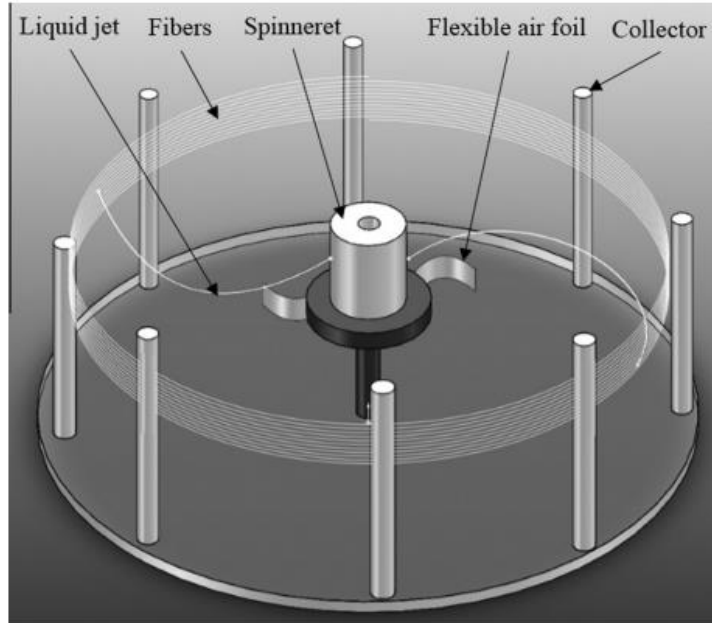


Figure 1.12. Schematic diagram showing a laboratory setup for centrifugal spinning.[51]

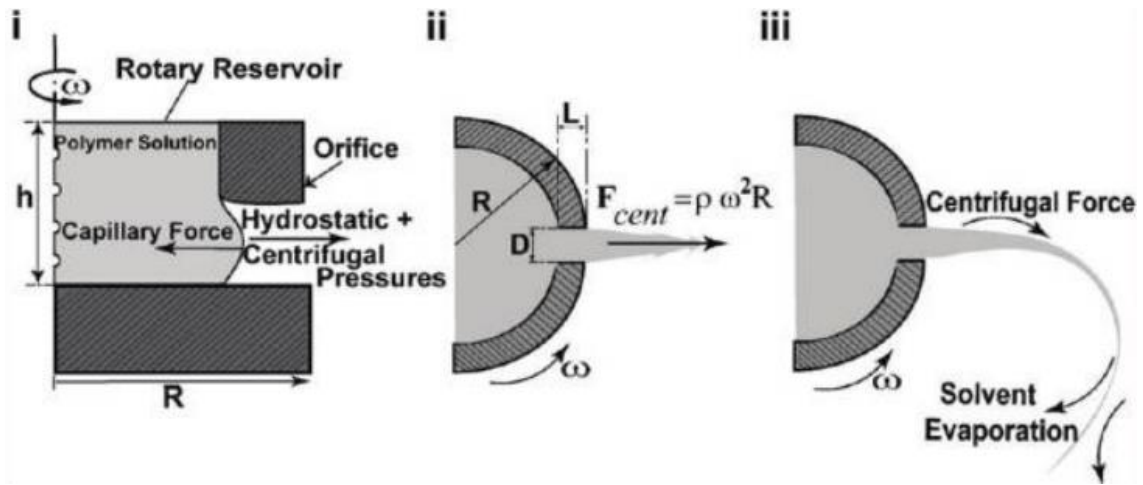


Figure 1.13. Schematic of nanofiber formation during centrifugal spinning: (i) jet-initiation, (ii) jet-extension, (iii) solvent-evaporation.[50]

1.2.3.2 Impacting parameters

Parameters that impact the spinning process and the structure of the resultant nanofibers include spinneret angular velocity, orifice radius, polymer viscoelasticity (which includes viscosity and relaxation time of the material), solution surface tension, solvent evaporation rate, temperature and the nozzle-collector distance.[52]

1.2.3.2.1 Solvent evaporation

Volatility is defined as the capability of a liquid to be vaporized at room temperature and pressure. During centrifugal spinning, the solvent is evaporated as the jet is expelled. If the evaporation rate of the solvent is too low, the fibers may be converted into a thin film as they deposit on the collector. On the other hand, if the time of solvent evaporation is too short, the elongation process may be limited, without allowing the full extension of the polymer jet, leading to fibers with large diameters.

1.2.3.2.2 Rotating force

Two major forces involved in the centrifugal spinning are centrifugal force (F_{centri}) and friction force (F_{fri}). These two forces can be calculated by the following two equations:

$$F_{centri}=m\omega^2D/2 \quad (1.1)$$

$$F_{fri}=-1/2\pi C\rho A\omega^2D'^2 \quad (1.2)$$

where m is the mass of the fluid, ω the angular velocity of the spinneret, D the diameter of the spinneret, C the numerical drag coefficient, ρ the density of air, and D' the diameter of the trajectory path. Equation 1.1 describes the force experienced by polymer fluid within the

nozzle tip while Equation 1.2 describes the force experienced by polymer jet in the trajectory state. Centrifugal force needs to be controlled carefully because sufficient centrifugal force can prevent bead formation and jet break-up.[28, 52]

1.2.3.2.3 Viscosity

Viscosity of a fluid is the resistance to flow and directly influences the fiber morphology. Since higher viscosity is usually obtained at higher solution concentration, it is more convenient to tune solution concentration instead of viscosity. During centrifugal spinning, a critical solution concentration, entanglement concentration, must be exceeded to form nanofibers. When the polymer solution is too dilute (*i.e.*, viscosity is too low), the insufficient polymer chain entanglements makes it difficult to produce fibers and leads to bead formation. On the other hand, if the solution concentration is too high (*i.e.*, viscosity is too high), the centrifugal force may not be strong enough to stretch the jet into thin fiber. [51, 53]

1.2.3.2.4 Surface tension

The cohesive forces among liquid molecules are responsible for the phenomenon of surface tension. In the bulk of the liquid, each molecule is pulled equally in every direction by neighboring liquid molecules, resulting in a net force of zero. The molecules at the surface do not have other molecules and therefore are pulled inwards. This creates some internal pressure and forces on the gas side, causing the liquid surface to contract and form curvature

at the surface. As the jet is stretched, the surface tension of the polymer solution is tending to break the jet and produce beads. Thus, in order to expel and stretch a polymer liquid jet, the surface tension must be overcome by enough centrifugal force. In addition, increasing viscosity can also relieve the effects of surface tension.

1.2.3.2.5 Nozzle geometry

Decreasing the nozzle diameter is an effective approach in reducing the fiber diameter. Mo et al.[54] found that smaller nozzle diameters help alleviate clogging and bead formation during spinning. Extrudate swelling, which increases the jet diameter, can be explained by stress relaxation originated from the elastic component of the polymer.[6]

1.2.3.2.6 Nozzle-collector distance

The distance between nozzle tip and collector affects the liquid jet flight time and the evaporation of the solvent. In addition, it also affects the morphology of the resultant fibers. As the jet travels, it is important that it has enough time before reaching the collector so that most of the solvent is evaporated. If the evaporation of solvent is not sufficient, the collected fibers may form films instead of a fibrous structure.[55]

1.2.3.2.7 Other parameters

Other environmental parameters can also affect the fiber formation process of centrifugal spinning. With increase in temperature, the viscosity of the fluid decreases, this favors the

reduction of the fiber diameter and at the same time the formation of beads. Air flow in centrifugal spinning also helps assist the spinning process as well as the diameter control of the resultant fibers.[28] Salt-polymer-solvent relationships can also affect the properties of the centrifugally-spun fibers.[56]

1.2.4 Applications of centrifugally-spun nanofibers

In recent years, various kinds of polymer fibers have been prepared by centrifugal spinning and have been utilized in different areas. Smooth and defect-free poly(butylene terephthalate) nanofibers [57], polyvinylpyrrolidone (PVP)/poly(L-lactic acid) (PLLA) polymer blend fibers, poly-lactic-co-glycolic acid (PLGA) nanofibers, etc., have been fabricated by centrifugal spinning and their tissue regeneration efficacies have been investigated.[58, 59] Other polymer materials such as poly(ethylene oxide) (PEO), polystyrene (PS) and poly(methyl methacrylate) (PMMA) have been prepared by centrifugal spinning and applied as structural composite materials. Polypropylene (PP) nanofibers are difficult to make by conventional electrospinning process because it does not have a room temperature solvent. However, PP nanofibers have been successfully produced by centrifugal spinning.[48, 49]

Not only polymer nanofibers, ceramic nanofibers can also be produced by centrifugal spinning technique. Ren *et al.* prepared silica nanofibers by centrifugal spinning of tetraethyl orthosilicate (TEOS)/PVP in ethanol solution. External and internal morphological differences between partially and completely hydrolyzed centrifugally-spun silica nanofibers

were discussed.[47] Hollow silica nanofibers prepared by centrifugal spinning was also reported.[60]

Carbon nanotube (CNT)-reinforced nanofibers have also been prepared by centrifugal spinning.[61-63] By doping functionalized CNTs into PAN and PMMA polymer blend solutions, Lozano *et al.* obtained CNT-reinforced nanofibers with increased tensile strength, electrical properties and thermal shrinking properties. Figures 1.14 and 1.15 show SEM results of the CNT-reinforced PMMA nanofibers and the corresponding tensile stress-strain test results.

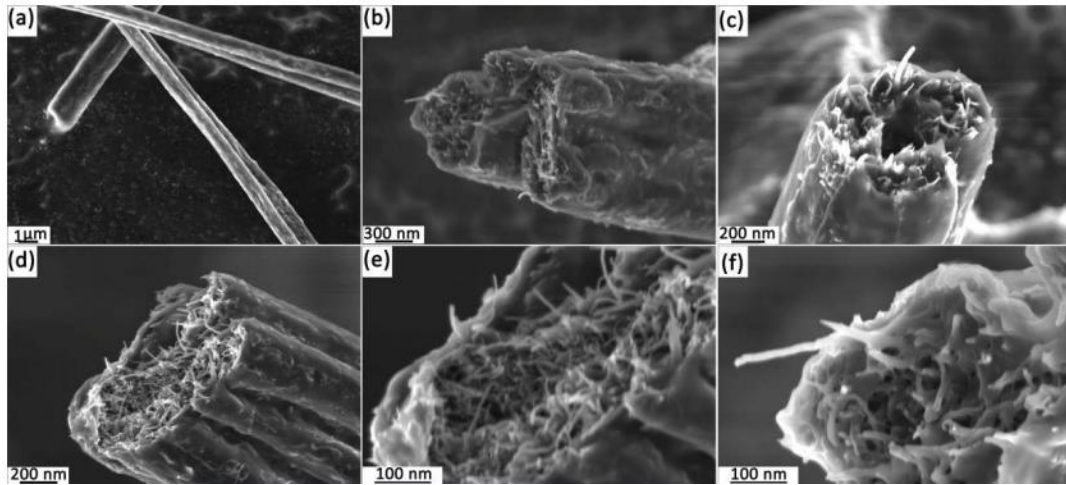


Figure 1.14. SEM images of 12wt% CNT/PMMA composite nanofibers.[62]

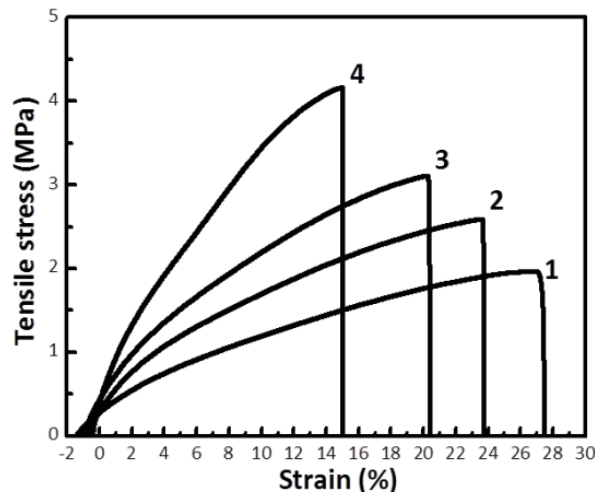


Figure 1.15. Tensile strength-strain curves of CNT/PMMA nanofibers with different CNT contents: (1) 0wt%, (2) 3wt%, (3) 8wt%, and (4) 12wt%. [62]

Energy-storage applications of centrifugally-spun nanofibers have been reported by Lozano et al. By combining vanadium oxide and polyvinylpyrrolidone precursor, they produced low cost, bendable vanadium oxide-filled carbon nanofibers for energy storage in lithium ion batteries. [64] Figure 1.16 shows the cyclic voltammetry (CV) curves of the flat electrode and roundup electrode, and the shape of the CV curves were not changed, indicating the good reversibility of the nanofiber electrode. The nanofibers also exhibited a reversible charge capacity of lower than 100 mAh g^{-1} under the current density of 100 mA g^{-1} , which indicates a large potential for performance improvement.

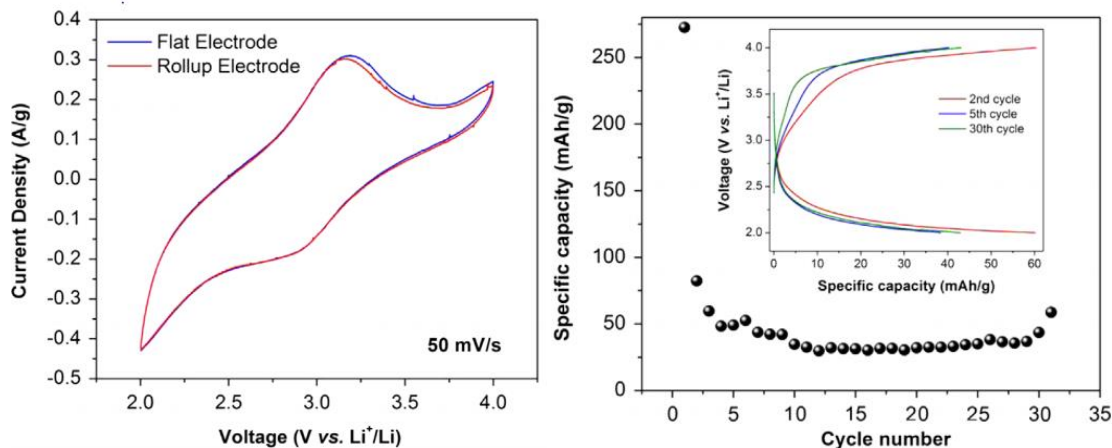


Figure 1.16. (A) Cyclic voltammetry curves, and (B) cycling performance of the vanadium oxide-filled carbon nanofibers. Inset in B shows the charge/discharge curves for the 2nd, 5th and 30th cycles. [64]

1.3 Carbon nanofiber based materials for lithium-ion-batteries

Renewable energy sources are playing a pivotal role in today's increasingly energy demanding society. Global warming, over consumption of fossil fuels, pressing demands for alternative energy source for electric vehicles/ hybrid electric vehicles all urge researchers to develop replacements for traditional energy resources.[65, 66]

In the past decades, rechargeable battery technologies have experienced spectacular advances. From traditional nickel-metal hydride (Ni-MH), lead acid to next generation rechargeable batteries such as lithium-ion batteries [14-16, 66-73], sodium-ion batteries [74-77], lithium-sulfur batteries [78-80], lithium-air batteries, and sodium-sulfur batteries [81, 82], new technologies provide better safety solutions, longer cycling life and higher volumetric and

gravimetric energy densities, etc. A comparison of different rechargeable battery systems is shown in the Figure 1.17.

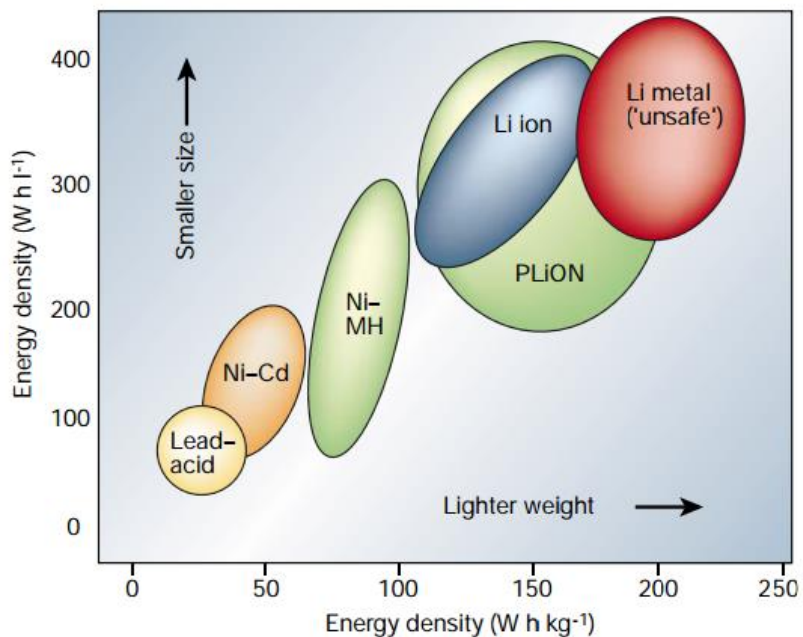
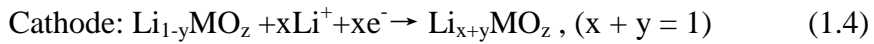


Figure 1.17. Comparison of the different battery technologies in terms of volumetric and gravimetric energy densities.[83]

1.3.1 Working principle

Lithium-ion batteries are mainly composed of four components: a positive electrode (cathode), a negative electrode (anode), a separator and an electrolyte. In general, lithium ions intercalate between cathode and anode during charge and discharge. On charging, Li^+ ions are deintercalated from the layered cathode host, transferred across the electrolyte, and intercalated into the anode. The discharge reverses this process in which the electrons pass

around the external circuit to power various systems (Figure 1.18).[84, 85] Therefore, the electrochemical charging-discharging process involves solid-state redox reactions, with the discharge process described as:



The charging process is the reverse of these equations.

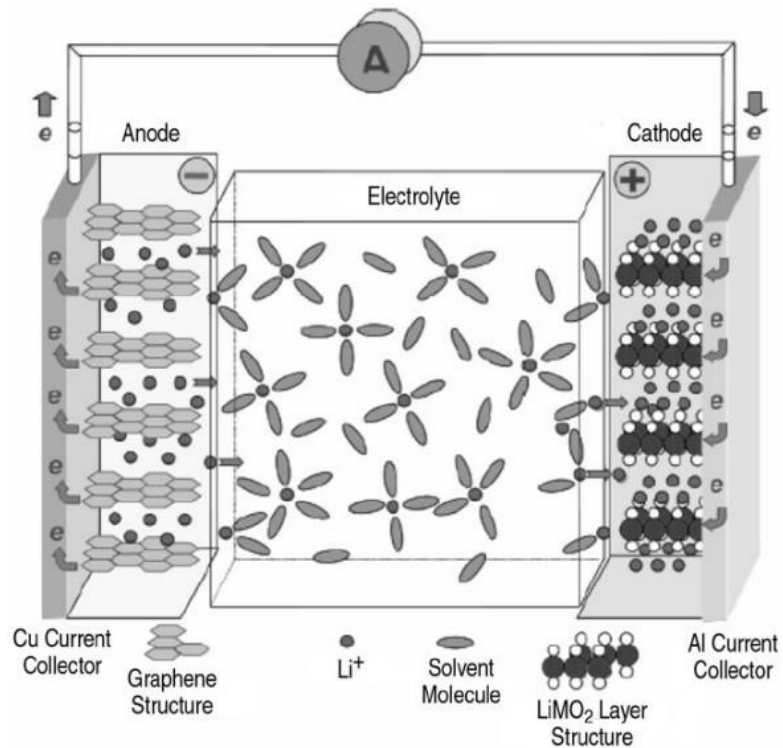


Figure 1.18. A lithium ion cell based on lithium-metal oxide cathode and graphite anode.[84]

1.3.2 Recent advances in anode materials

As aforementioned, lithium-ion batteries are promising candidate to replace traditional batteries. However, the ever-increasing electronic vehicle industry requires batteries bearing with longer cycling life, higher energy density and power density, and better environmental compatibility. Therefore, lithium-ion batteries with superior performance must be developed before they can be scaled up industrially. The key components of lithium-ion batteries are cathodes and anodes. On the commercial basis, cathodes are mainly made from lithium-ion host materials possessing high positive redox potentials. Examples are lithium metal oxides such as LiCoO_2 [86], spinels such as LiMn_2O_4 [87], and the lithium metal phosphates such as LiFePO_4 [88]. These cathode materials have relatively stable cycling performance but low capacities. On the other hand, anode materials show higher specific capacities compared to cathode materials, however, they suffer from relatively poor cycling stability. Thus, the major task for anode materials is to enhance their cycling performance.

1.3.2.1 Graphenes

Graphene is basically a two-dimensional sheet of sp^2 -hybridized carbon with a thickness of one atom. Its extended honeycomb network is the basic building block of other carbon allotropes; for example, it can be stacked to form 3D graphite, rolled to form 1D nanotubes, or wrapped to form 0D fullerenes.[89] Graphene has a considerable Li-storage ability since Li can be adsorbed not only on both sides of graphene sheets, but also on the edges, defects, disorders, and covalent sites of graphene nanoplatelets.[65] The major disadvantages of

graphene anodes are their high irreversible capacity, poor cycling performance and lack of voltage plateau.

Graphenes anchored with active metal and/or metal oxide nanoparticles can be used to reduce the irreversible capacity and enhance the cycle life.[90, 91] Several factors contribute to the enhanced performance of the metal/metal oxide anchored graphene: large Li storage of the active materials, good electrical properties of the graphene, volume suppressing effect of the graphene, and good structural stability.

1.3.2.2 Graphites

Graphite is by far the most commercially successful anode material because of its low and flat working potential, long cycle life, low cost and low volume expansion. Graphite is featured as a stack of hexagonally bonded sheets of carbon held together by van der Waals forces. The forces between any two given carbons in the same sheet (which share sp^2 hybridized bonds) are much stronger than the forces between any two concurrent sheets. As a result, Li^+ ions are able to be inserted in between the planes of graphite. Though a stoichiometry of LiC_6 (372 mAh g^{-1}) can almost be reached (Figure 1.19) [92], only a limited energy density can be produced for graphite anodes. Furthermore, the Li ion transport rates of graphite are less than $10^{-6} \text{ cm}^2 \text{ s}^{-1}$. Since the chemical diffusion coefficient of Li^+ is related to the power density of the battery, graphite suffers from a low power density.[65, 93]

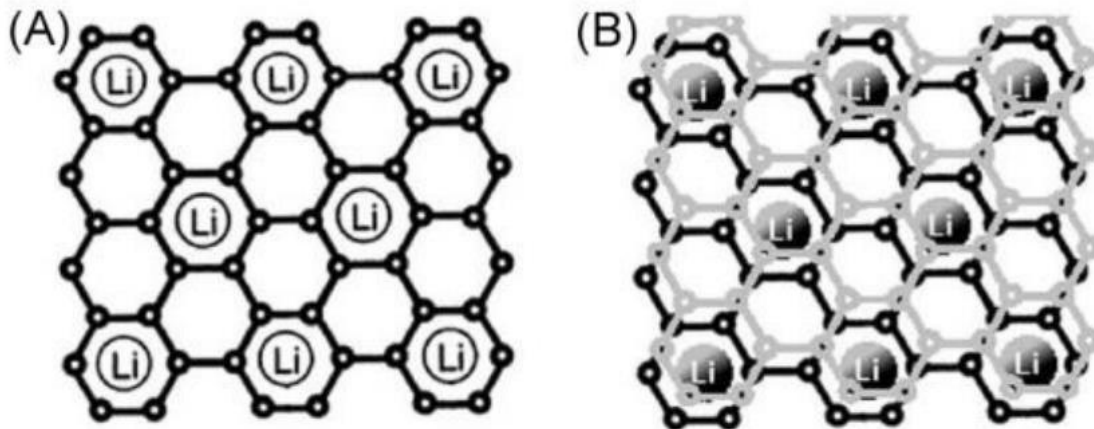


Figure 1.19. Schematic of lithium intercalation in graphite: (A) lithium is inserted in every second carbon hexagon and (B) between the graphite layers.[92]

1.3.2.3 Carbon nanotubes

As an allotrope of graphite, carbon nanotubes (CNTs) have been proved to be a promising candidate for anode materials due to their unique properties: high conductivity, high aspect ratio, high activated surface, low density and ideal mechanical properties.[94, 95] It has been demonstrated that the reversible capacities of single-walled CNTs and multi-walled CNTs can be as high as 400-600 mAh g⁻¹ or even up to 1000 mAh g⁻¹, [96-98] due to reversible intercalation with graphitic layers, and adsorption or accumulation of Li ions in defect area.

Choi et al. recently reported multi-walled CNT-based anode material for lithium-ion batteries. Figure 1.20 shows the electrochemical performance of the multi-walled CNTs grown on copper foils. Figure 1.20.a shows the first two charge-discharge curves. At first cycle, a specific discharge capacity of 2500 mAh g⁻¹ and charge capacity of 1455 mAh g⁻¹ were achieved at a current rate of 0.1 C, assuming theoretical capacity same as graphite. A voltage

plateau between 0.5-0.9 V was observed due to SEI formation on CNTs surface.[99] Rate performance was shown in Figures 1.20.b. and 1.20.c. The reversible capacity of the electrode was found to be very high and quite stable, and even at high charging/discharging rate of 3.0 C, the electrode showed a reversible capacity of 767 mAh g⁻¹. Over 99% of the Coulombic efficiency was observed after the first two cycles at 1.0 C rate.[96]

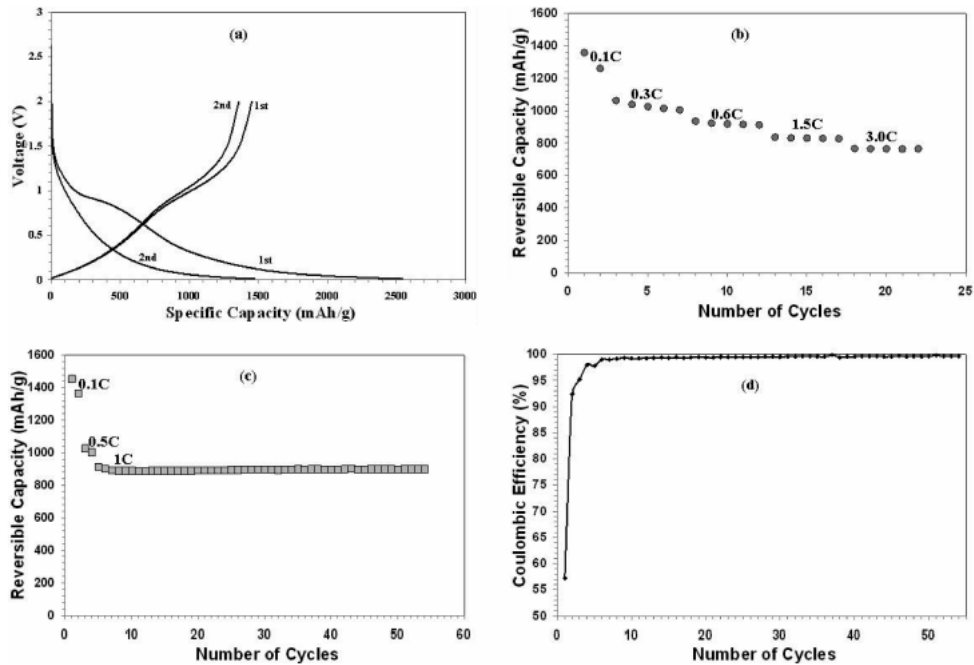


Figure 1.20. Charge-discharge curves (a), rate performance (b), cycling performance (c), and coulombic efficiency (d) of CNT anodes.[96]

The advantages of CNTs compared to graphite are obvious. CNT anodes have excellent mechanical properties, which can help accommodate dramatic volume expansion caused by

metal active materials. This is important because it enables the use of high-capacity metal active materials in anodes.[92]

However, challenges still remain. The mass production of CNTs is rather difficult, because parameters such as diameters, surface functionality, number of graphene monolayers, length, degree of defects, textures and electronic properties are still hard to control. In addition, CNTs lack a voltage plateau while the battery is discharging, and this makes them difficult to be used in most electronics which require a stable voltage source. Currently, the only commercial use of CNTs is additives or fillers for electrode materials.

1.3.2.4 Carbon nanofibers

Carbon nanofibers (CNFs) are one-dimensional nanomaterial with diameters ranging from 10 nm to 1000 nm, and length ranging from 0.5 μm to 100 μm . CNFs are considered as an intermediate between carbon nanotubes and normal carbon fibers, and their structures are composed of the stacks of small graphene basic units. CNFs are featured by high tensile strength (12,000 MPa) and high Young's modulus (600 GPa).[100] At the same time, CNFs also possess good electric conductivity, which makes them ideal for energy storage applications.

Several methods have been utilized to fabricate carbon nanofibers. For example, chemical vapor deposition uses hydrocarbon compounds as starting materials, followed by thermal treatments (500 $^{\circ}\text{C}$ -1000 $^{\circ}\text{C}$) to grow nanofibers under catalyst particles.[101-103] However,

the dominating approach currently is electrospinning. With thermal treatments, electrospun polymer precursor nanofibers can be used to form carbon nanofibers. PAN is often chosen as the precursor to make CNFs due to its high carbon yield. Two heat treatment steps are involved in the process of converting PAN to carbon. The first heat treatment step, stabilization, is done at 250-300 °C in air, during which PAN becomes a cross-linked structure through dehydrogenation and cyclization reactions. The second thermal treatment step, carbonization, is performed in an inert atmosphere (e.g. nitrogen or argon) at 600-1300 °C, during which most non-carbon elements are removed in the forms of methane, hydrogen, hydrogen cyanide, water, carbon dioxide, and ammonia, etc.[104] Typical stabilization and carbonization processes of PAN fibers are shown in Figure 1.21.

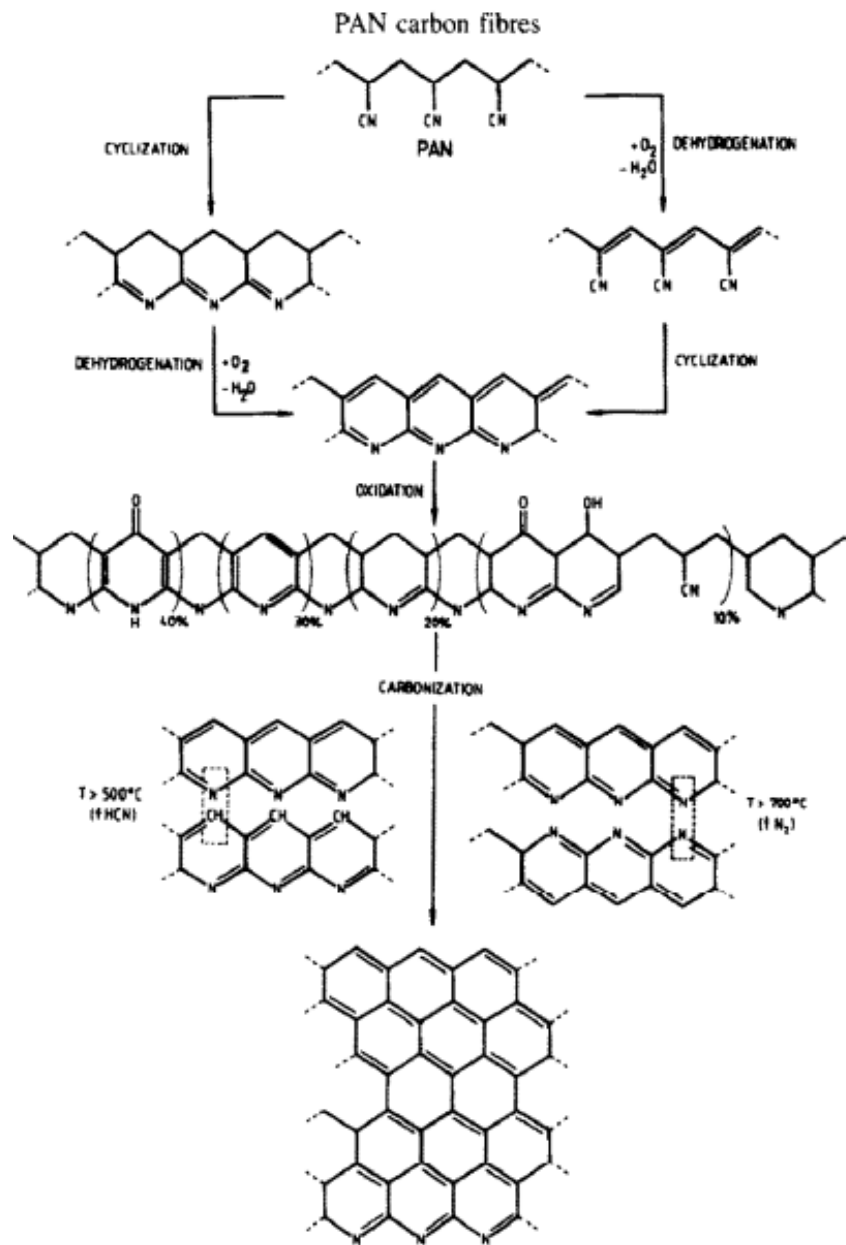


Figure 1.21. Mechanisms of the stabilization and subsequent carbonization of PAN.[104]

The resultant CNFs can undergo additional heat treatments up to 3000 °C for further graphitization. Due to excellent electric, mechanical and thermal properties, CNFs have found applications in areas such as energy storage, biomedicine, protective clothing, filtrations, etc.[105, 106]

1.3.3 Carbon group alloying elements and composites

Elementary substances from carbon group (tetrels) such as silicon (4200 mAh g^{-1}), germanium (1600 mAh g^{-1}) and tin (990 mAh g^{-1}) provide promising alternatives to conventional carbonaceous anode active materials due to their high theoretical capacities. However, these anode materials suffer from dramatic volume expansion, which causes cracking, crumbling or even pulverization during cycling, leading to poor cycling stability.[70, 107]

To address the cycling stability issue, various solutions have been proposed to alleviate the side effects of these potential anode materials. For example, Yushin et al. [108] used cheap carbon black as substrate material to anchor chemical vapor grown silicon nanoparticles (Figure 1.22). In addition to carbon black, graphenes [90, 109], CNFs [14, 15, 73, 110, 111] and CNTs [16] were also introduced as carbonaceous matrix. Lake and coworkers used CVD to deposit silicon into CNFs.[112] Figure 1.23 shows the SEM characterization of the resultant silicon/CNF composite. A uniform coverage as sub-20 nm silicon nodules was observed decorating both the interior and exterior of the CNF surfaces.

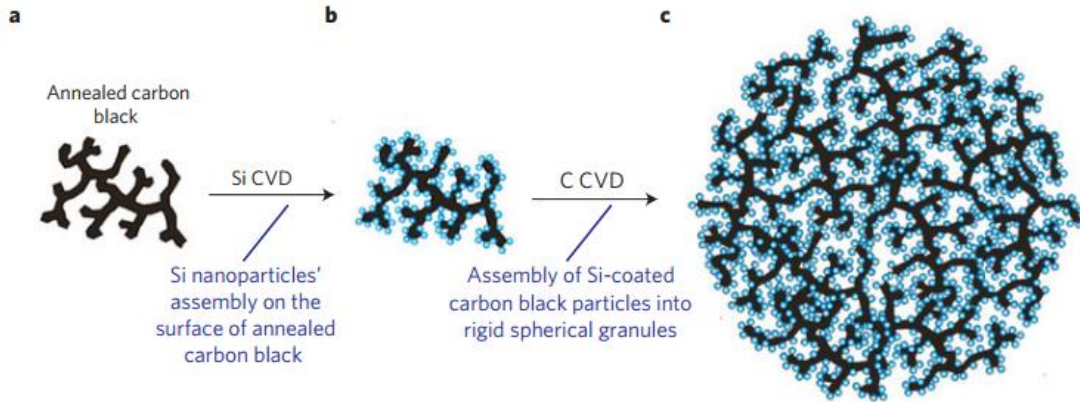


Figure 1.22. Schematic of Si–C composite assembly. a–c, Annealed carbon-black dendritic particles (a) are coated by Si nanoparticles (b) and then assembled into rigid spheres with open interconnected internal channels during C deposition (c).[108]

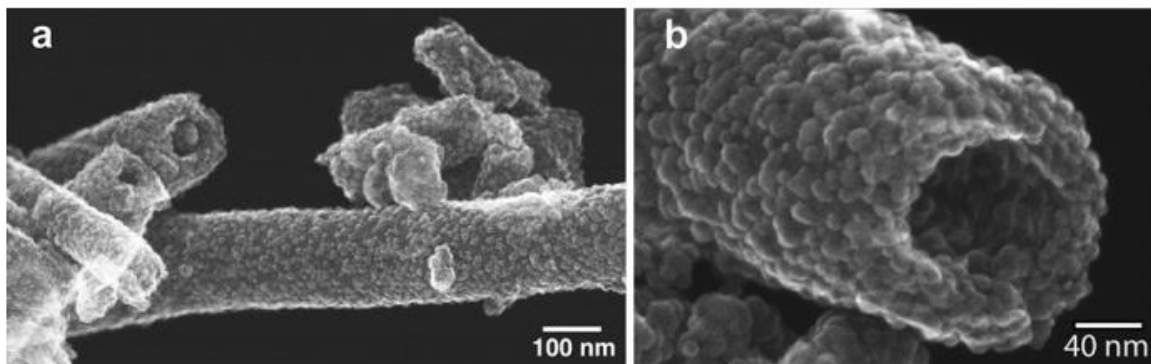


Figure 1.23. SEM images of the silicon/CNF composite: uniformly distributed nanosized Si nodules on the exterior and interior surface of CNFs.[112]

Recently, Li et al. used vertically-aligned CNFs as substrates and grew silicon layers upon them by CVD. They claimed this structure could effectively accommodate the volume expansion/contraction of Si in the radial direction during charge-discharge cycles. The short path of Li^+ transport across the thin Si shell allows a much higher charge/discharge rate and

significantly improved power density. Figures 1.24 and 1.25 demonstrate the structure design of this work and the achieved cycling performance.[113]

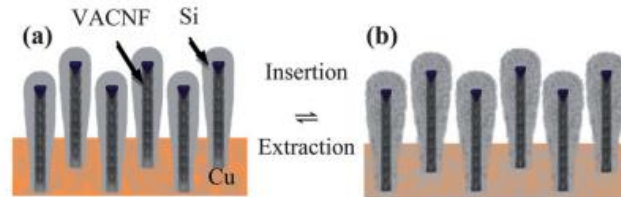


Figure 1.24. Schematic illustration of the reversible structural changes of the coaxially coated Si on vertically aligned CNFs in (a) extracted (discharged) and (b) inserted (charged) states.[113]

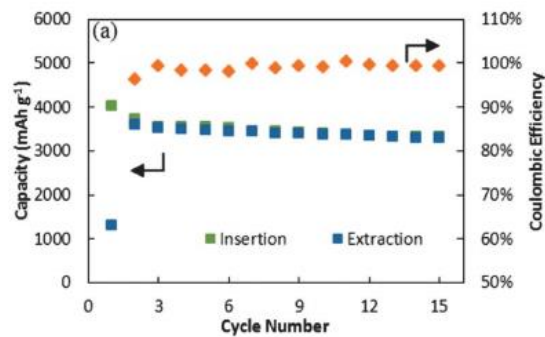


Figure 1.25. Cycling performance of a 10 mm long vertically aligned CNF array coated with 0.5 μm Si.[113]

Zhi et al. explored different contact modes between carbon and active materials.[114] It was found that the 1-D/1-D hybrid structure held the robust line-to-line contact between Si and C, which created efficient channels for the fast transport of both electrons and lithium ions during cycling.

In addition to the extensively studied silicon, metallic tin has also been demonstrated to be a promising candidate for use in anodes. Firstly, its theoretical specific capacity ($\text{Li}_{4.4}\text{Sn}$, 992 mAh g^{-1}) is much higher than that of graphite (LiC_6 , 372 mAh g^{-1}). Secondly, tin has higher operating voltage than graphite, and hence it is less reactive and the safety of batteries during rapid charge/discharge could be improved.[115] Yu et al. improved the electrochemical performance of electrospun Sn-C electrodes by forming metallic tin particles encapsulated in porous multichannel carbon microtubes. The motivation to fabricate porous structure was to reach an appropriate balance between the high packing density of Sn particles and sufficient space to buffer the volume expansion.[116, 117] Schematic of the fabrication process and electrochemical performance are shown in Figures 1.26 and 1.27 These Sn-C electrodes maintained a stable capacity greater than 600 mAh g^{-1} during cycling.

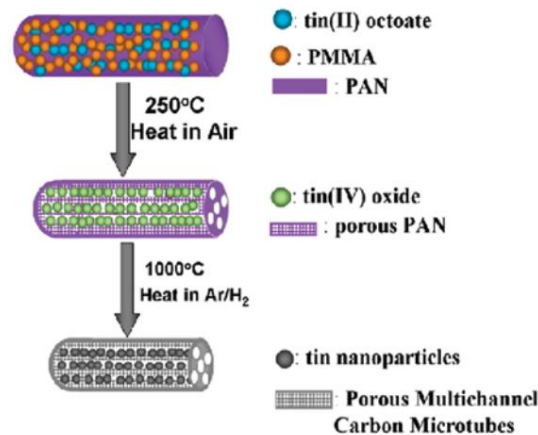


Figure 1.26. Schematic for preparing porous multichannel carbon microtubes containing Sn nanoparticles.[116]

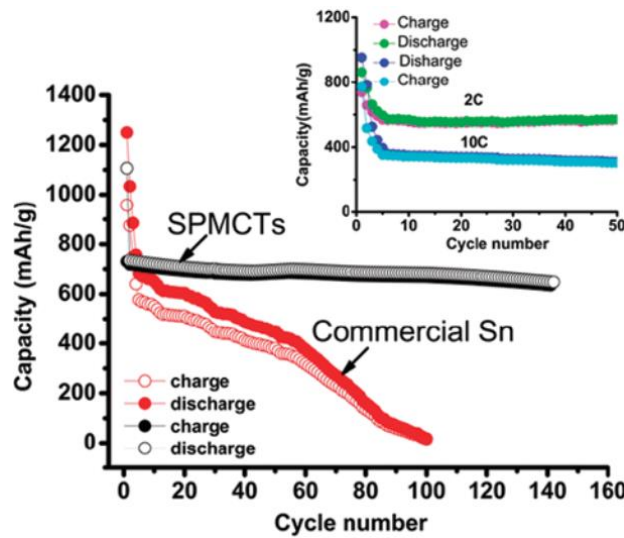


Figure 1.27. Cycling performance of Sn encapsulated in porous multichannel carbon microtubes (SPMCT) and commercial Sn. The inset displays the discharge capacities of SPMCT electrodes at 2 and 10 C.[116]

In 2010, Huang et al. reported Sn/C non-woven film prepared by electrospinning and carbonization treatment.[118] Figure 1.29 (Left) shows the charge-discharge curves of the Sn/C non-woven film. The reversible charge capacity of the Sn/C non-woven film in the 1st, 10th and 20th cycle was 395, 392 and 382 mAh g⁻¹, respectively. Figure 1.29 (Right) shows the cycling performance of Sn/C non-woven film. The reversible capacity remained 96.7% after 20 cycles.

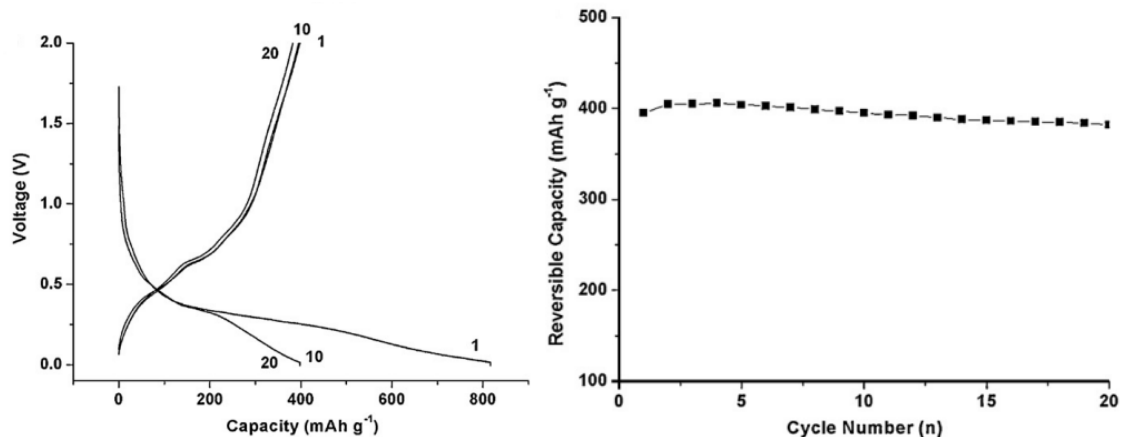


Figure 1.28. (Left) Charge-discharge performance (Right) cycling performance of Sn/C non-woven films. [118]

Kang et al. fabricated a film of porous carbon nanofibers containing Sn/SnO_x nanoparticles in the pores by introducing freezing and carbonization process after electrospinning. The as-prepared film has tin/tin oxides encapsulated in porous carbon nanofibers. The frozen water was used to create two phases which are PVA and the ice of SnCl₂ containing water mixture. After that, frozen fibers were carbonized, during which water was evaporated and pores were formed in the substrate. Meanwhile, SnCl₂ was decomposed and reduced to Sn/SnO_x and then grew up to form particles, which were encapsulated in the pores.[119] Figures 1.29 and 1.30 show TEM characterization results and the electrochemical performance of the Sn/SnO_x based carbon nanofiber composite.

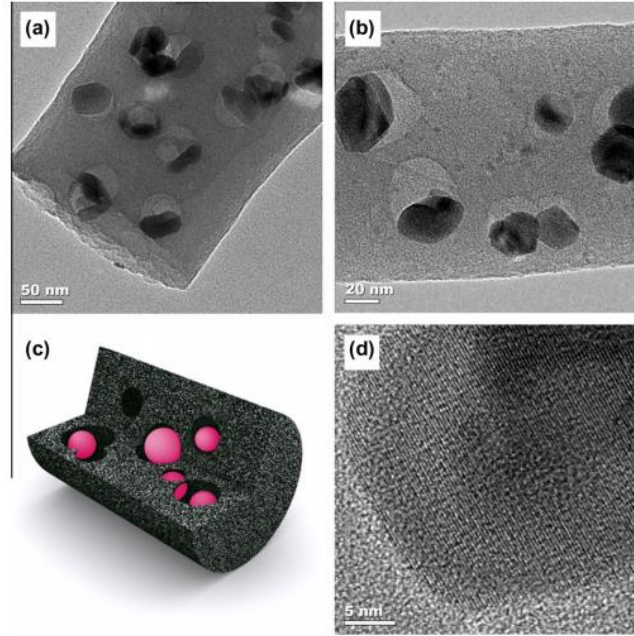


Figure 1.29. TEM images (a,b), microstructures (c), and HRTEM image (d) of the tin/tin oxides encapsulating porous carbon nanofibers.[119]

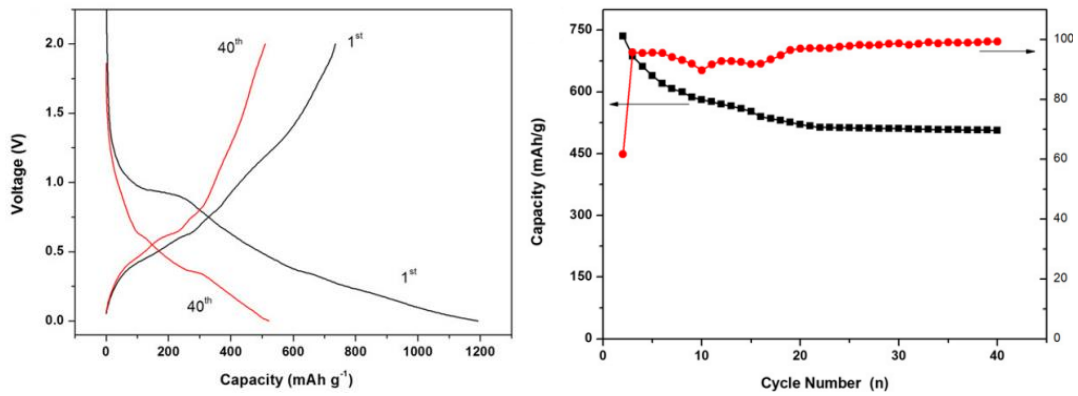


Figure 1.30. Charge/discharge profiles (left) and cycling performance (right) of the tin/tin oxides encapsulating porous carbon nanofibers.[119]

Challenges related to Sn/C nanofibers still persist although modifications such as chemical vapor deposition carbon coating have been used to increase the coulombic efficiency, acting as a physical buffer to prevent direct contact from electrolyte to active materials.[120] Limited stability due to Sn nanoparticle agglomeration or Sn-catalyzed electrolyte decomposition remains a problem.[121] In particular, this problem becomes more challenging at high current densities, where a significant amount of thermal energy is present to accelerate the diffusion of Sn.[122]

1.4 Supercapacitors

Supercapacitor, a generic term for a family of electrochemical capacitors, includes electric double-layer capacitor (EDLC), pseudocapacitor and hybrid capacitor.[123] An EDLC is a device that stores charge electrostatically via reversible adsorption of ions of the electrolyte onto the surface of electrode materials.[124] Different from lithium-ion batteries, supercapacitors are featured by their high power density and long cycle life. The Ragone plot shown in Figure 1.31 illustrates the differences between different energy storage systems. It is seen from Figure 1.31, EDLC possesses higher specific power up to 10^4 W/Kg compared to other systems such as lithium-ion batteries, sodium-sulfur batteries and Pb-acid batteries.

Supercapacitors, due to high power density and long cycle life, are widely applied in high power demanding devices such as regenerative braking, load leveling systems and accelerating systems in vehicles.[125, 126]

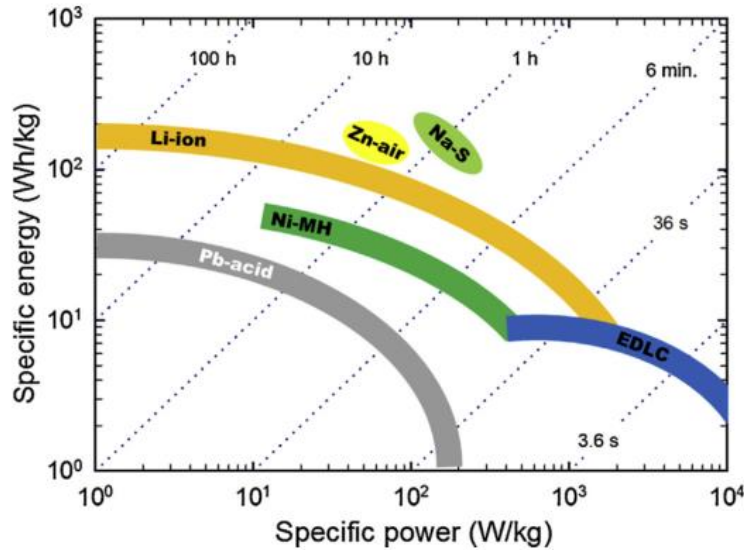


Figure 1. 31. Comparing power sources: energy versus power densities (Ragone plot).[126]

1.4.1 Working principle

A supercapacitor is composed of a pair of polarizable electrodes that are physically separated by a porous membrane through which ions can diffuse. Figure 1.32 shows a schematic of a symmetric supercapacitor. A typical electric double layer capacitor is composed of a pair of electrode, electrolyte, an ion permeable separator and a pair of current collector. The capacitance of a supercapacitor is assumed to follow that of a parallel-plate capacitor:

$$C=(\epsilon_r\epsilon_0/d)A \quad (1.5)$$

where ϵ_r is the electrolyte dielectric constant, ϵ_0 the permittivity of a vacuum, A the specific surface area of the electrode accessible to the electrolyte ions, and d the effective thickness of the EDL (the Debye length).[124] The very small d and very big A value of EDLC contribute

to the storage of hundreds or thousands of times more charges than solid-state and electrolytic capacitors. The energy (E) of a supercapacitor can be calculated by using:

$$E = \frac{1}{2}CU^2 \quad (1.6)$$

where C is the capacitance in Farads, and U the operating voltage. The power (P) of a supercapacitor can be calculated by using:

$$P = \frac{U^2}{4R_s} \quad (1.7)$$

where R_s is the equivalent series resistance of the supercapacitors. Other than electrostatic approach of charge-storage mechanism, pseudocapacitance may also contribute to capacitive energy storage. Different from electrostatic approach, pseudocapacitance arises from reversible redox reactions occur at or near the surface of an appropriate electrode material, which leads to much greater charge storage.[127]

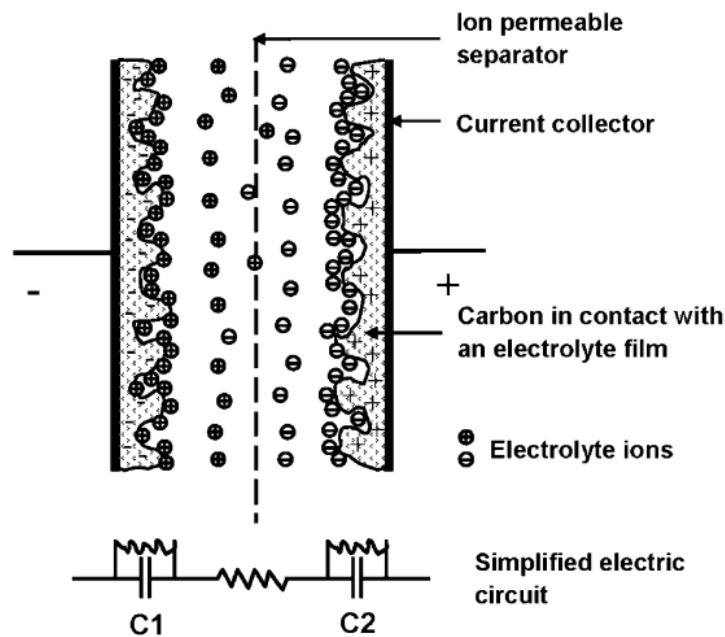


Figure 1.32. Schematic illustration of an electric double layer capacitor.[128]

1.4.2 Impacting factors and electrode materials

The microstructure of electrode materials dominates the capacitive performance of supercapacitors. Important microstructural characteristics include active layer thickness, specific area and pore characteristics.

Carbon-based supercapacitors are EDLCs, where the storage of energy is accomplished by electrostatic charge accumulation at electrode/electrolyte interfaces. Thus, EDLCs are featured by stable cycling performance and high power density.

Pore size and surface area play dominant role in determining the electrochemical performance of EDLCs. Porous electrodes can be categorized into three types: 1) micro- (<2nm), 2) meso- (2-50nm), 3) macropores (>50nm).[129]

The BET surface area plays a crucial role in the electrical double layer charge storage. High surface area guarantees more available sites for ions to be accumulated by electrostatic interactions. It should be noted that that high BET surface area does not guarantee high specific capacitance. Figure 1.33 illustrates the ion size and pore size effect on nanoporous carbon electrode, and it is observed that small pores block the ions from penetrating the pore, preventing fully utilization of the surface area, while a suitable pore size facilitates the ion migration to form EDLCs.[126] In aqueous electrolyte medium, the effective ionic dimension of cations, such as Cs^+ , K^+ , Na^+ , and Li^+ , is less than 0.42 nm and that of anions, such as NO_3^- , Cl^- , F^- , Br^- , is less than 0.51 nm.[130]

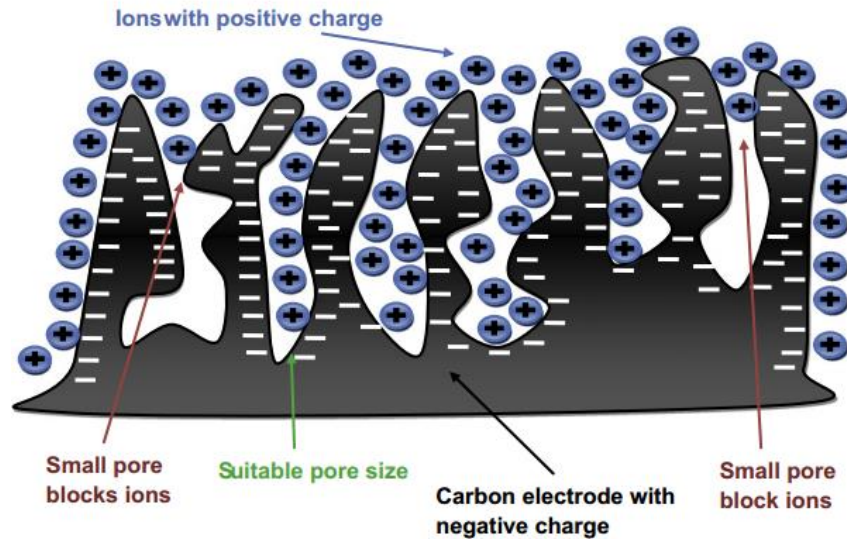


Figure 1.33. Schematic of the ion size and pore size effect on nanoporous carbon electrode.[126]

Y.H.Lee et al. proposed the relations between BET surface area, pore diameter and specific capacitance (Figure 1.34) and relations between mesopore, micropore and specific capacitance (Figure 1.35).[131] From Figure 1.34, it is observed that when pore diameter is a fixed parameter, larger BET surface areas result in higher specific capacitance values. On the other hand, for a fixed BET surface area, higher capacitances were observed for smaller micropores. From Figure 1.35, it can be concluded that with a fixed mesopore volume, the capacitance performance deteriorates with the decreasing micropore volume, while high mesopore volume results in poor capacitance performance. Thus, it can be concluded that an optimal combination of BET surface area and pore structures is pivotal in electrode design for supercapacitors.

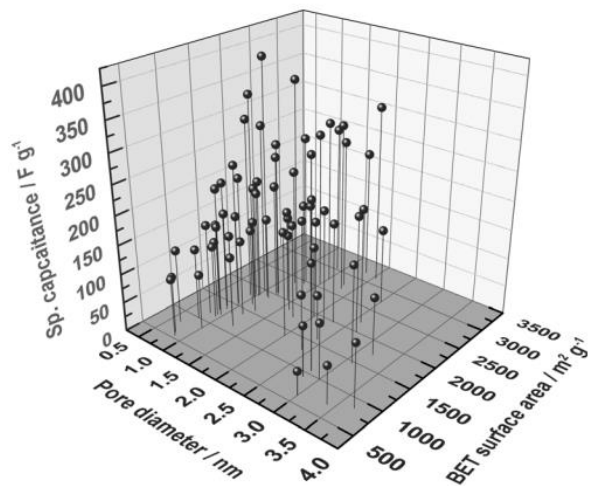


Figure 1.34. The dependence of specific capacitance on pore diameter and BET surface area.[131]

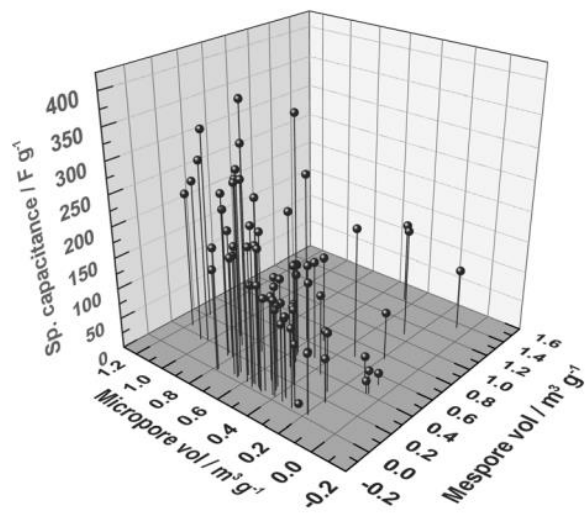


Figure 1.35. The dependence of specific capacitance on micro- and mesopore volumes.[131]

To date, various forms of carbon materials such as activated carbons [132], carbon nanotubes [133], carbon aerogels [134], graphene sheet [135, 136], CNFs [106, 137, 138] and various carbon-based composites, mostly combine carbon with pseudocapacitive materials (metal oxide and conducting polymers) together, have been widely investigated.[139-141]

F.Beguin and coworkers prepared activated PAN-based CNF papers at temperatures from 700 to 1000 °C and used them as supercapacitor electrode.[142] Figure 1.36 shows the cyclic voltammetry results for CNFs activated at 900 and 1000 °C. It can be observed that although the BET specific surface area of the CNFs activated at 900 °C ($376 \text{ m}^2 \text{ g}^{-1}$) is half of that for the CNFs activated at 1000 °C ($705 \text{ m}^2 \text{ g}^{-1}$), the capacitances of the two materials are comparable and independent of the electrolyte.

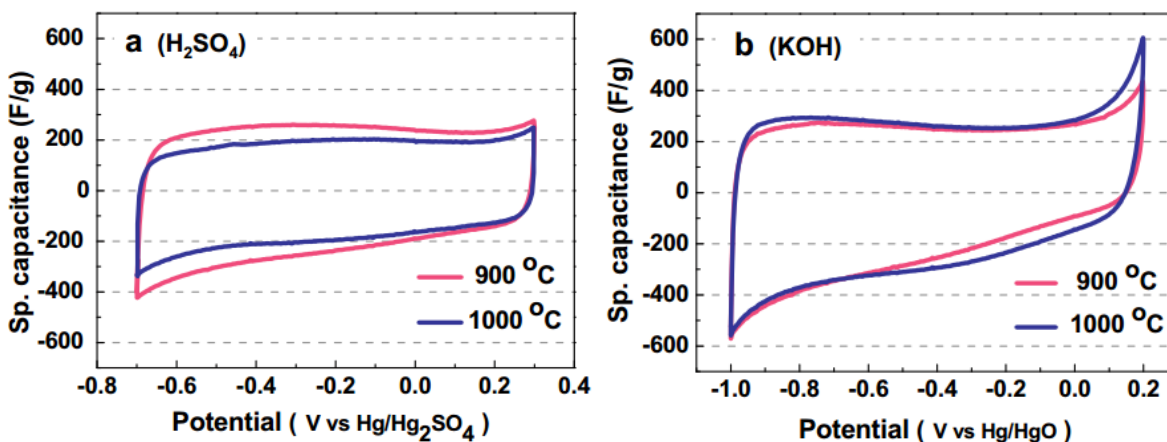


Figure 1.36. CV curves of the 900 °C and 1000 °C carbonized/activated samples at a scan rate of 2 mV/s in (a) 1 mol L⁻¹ H₂SO₄ and (b) 6 mol L⁻¹ KOH.[142]

CHAPTER 2 OBJECTIVES

The main objectives of the work are to explore centrifugal spinning as a high-production rate, facile-to-handle nanofiber fabrication method and study centrifugally-spun nanofibers' potential energy storage applications ranging from anode materials for lithium-ion batteries to high-surface area electrodes for supercapacitors. The work includes:

1. Centrifugally-Spun Tin-Containing Carbon Nanofibers for Use as Anode Material for Lithium-ion Batteries

Integrating active materials such as tin and silicon into carbonaceous matrix materials such as CNFs provides superior electrochemical performance compared to traditional anode materials. On one hand, active materials can provide high specific capacities; on the other hand, CNFs can act as confinement material to accommodate the volume expansion and prevent subsequent pulverization.

However, CNFs, as a crucial category of electrode materials, have been prepared mainly by electrospinning. The low-production rate of electrospinning limits its up-scaling production, and the complexity of large-scale electrospinning devices largely confines the application of nanofibers. Herein, we fabricated precursor fibers via centrifugal spinning and produced tin-containing CNFs by subsequent thermal treatments. The composite was then used as anode materials in lithium-ion batteries.

2. Fabrication of Centrifugally-Spun Carbon Nanofibers and Their Application as Electrode Material for Supercapacitors

High-surface area carbon materials attract enormous interest due to their versatile applications ranging from catalysis, energy storage, sensors, and filtration. Conventional processes for producing high-surface area carbon materials require a pore-creation step, which involves complex and costly chemical and physical reactions. Template method has been investigated as an alternative for producing pores with sizes from nano to micro-scale. However, difficulties such as template design and carbon growth still remain as problems. An alternative approach to produce high-surface area nanofiber is to spin immiscible polymer blends, followed by thermal treatments.

Herein, we used centrifugal spinning to produce nanofibers from a blend of polyacrylonitrile and polymethyl methacrylate. After thermal treatments, high-surface areal CNFs were fabricated and used as supercapacitor electrodes.

CHAPTER 3 CENTRIFUGALLY-SPUN TIN-CONTAINING CARBON NANOFIBERS AND THEIR APPLICATION AS ANODE MATERIAL FOR LITHIUM-ION BATTERIES

Abstract: By far, CNFs have been mainly produced by electrospinning of precursor fibers with subsequent heat treatment. The low-production rate of electrospinning confines the up-scaling production and practical application of CNFs prepared by electrospinning. Recently, centrifugal spinning has drawn extensive attention due to its high production rate (500 times faster than traditional electrospinning), easy operation and simple set-up. CNFs can be prepared by centrifugal spinning of precursor polymer nanofibers, followed by thermal treatment. The electrochemical performance of these CNFs can be enhanced by integrating active materials. Herein, tin-containing CNFs were prepared by centrifugal spinning of the tin salt-PAN precursor fibers and subsequent thermal treatment. Polymer-salt-solvent relationships and their effects upon viscosity were discussed, and the use of tin-containing CNFs as anode material in lithium-ion batteries was explored.

Keywords: Centrifugal spinning, composite nanofiber, CNFs, tin, lithium-ion batteries.

3.1 Introduction

Among various energy storage solutions, lithium-ion batteries are currently the most promising candidate for applications ranging from portable electronics to electric vehicles, due to their high energy density, long cycle life, good rate performance and low environment impact.[66, 117] As one of the key components of lithium-ion batteries, anode plays a major role in the development of this cutting-edge technology. The most commercialized anode material, graphite, exhibits low specific capacity and can hardly meet the increasing demands of newly-developed technologies such as hybrid-vehicles and sustainable energy storage. On the other hand, active materials, such as silicon, tin, and germanium, suffer from large volume expansion during charge-discharge cycles, which leads to unsatisfactory cycling performance. Impressive advancements have been achieved by integrating high-capacity active materials into CNFs.[14, 15, 120, 143] Dispersing nano-size active materials into CNF matrix can not only accommodate the dramatic volumetric expansion of active materials during lithiation/delithiation [144], but also maximize the capacity potential of active materials by preventing the nanoparticle pulverization or the loss of contact between active substances and the current collector.[145]

Currently, the precursor fibers for CNFs are mainly prepared by electrospinning, a time-consuming method with a low production rate of 0.1-1 g/h per nozzle.[146] Although modified needle-less electrospinning such as patented NanospiderTM technique has been developed, [147] drawbacks such as labor-intensity, poorly-controlled nanofiber qualities [148] and complexity of the facility [149] still persist. Centrifugal spinning recently attracts

attention due to advantages such as simple set-up and high-production rate (>0.1 g/min per nozzle) compared to electrospinning.[48, 49] Figure 3.1 shows the schematic of a basic centrifugal spinning machine and the nanofiber fabrication process. Centrifugal force, exerted from high-speed rotary spinneret, is applied during the centrifugal spinning. Spinning solutions will be ejected from nozzles and travel in a trajectory curve as long as centrifugal force can overcome the surface tension of the solutions.

Herein, we prepared tin-containing CNFs by the centrifugal spinning of tin salt/PAN precursor fibers and subsequent thermal treatment. Salt-polymer-solvent interactions were first investigated and then utilized to optimize parameters to fabricate suitable centrifugally-spun tin-containing CNFs for lithium-ion battery anode. Electrochemical results suggest tin-containing CNFs prepared by centrifugal spinning are promising anode material candidate for lithium-ion batteries.

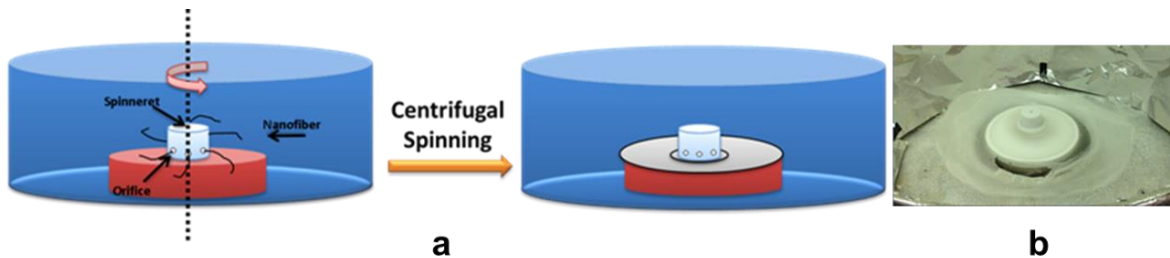


Figure 3.1. a) Schematic of centrifugal spinning machine setup, and b) the real-time photo of centrifugal spinning process.

3.2 Experimental

3.2.1 Materials

Polyacrylonitrile (PAN, Pfaltz & Bauer Inc., 150,000 g mol⁻¹), tin (II) chloride (SnCl₂, Aldrich), and N,N-dimethylformamide (DMF, Aldrich) were used as purchased.

3.2.2 Centrifugal spinning and thermal treatment

SnCl₂ salt (2, 5 and 8 wt% with respect to solution) were added into 15 wt% PAN solution in DMF and mechanically stirred at 90 °C for 24 h. Tin salt/PAN precursor fibers were produced by centrifugal spinning at a rotation speed of 3500 rpm. The spinneret had a cylindrical shape with 2 cm in height, 1.5 cm in radius and a nozzle diameter of 0.4 mm. Centrifugally-spun PAN/SnCl₂ nanofibers were stabilized in air environment at 280 °C for 5.5 h with a heating rate of 5 °C min⁻¹ and then carbonized at 700 °C for 2 h in argon atmosphere with a heating rate of 2 °C min⁻¹, during which PAN was pyrolyzed to carbon and SnCl₂ was reduced to Sn particles. The resultant Sn/carbon nanofibers were then used as the anode material for lithium-ion batteries.

3.2.3 Structure characterization and electrochemical evaluation

Viscosity and surface tension of the precursor solutions were measured to evaluate the spinnerability. During the viscosity measurements, pure DMF and SnCl₂/PAN solutions were loaded into the viscometer (ATS Rheosystem) fitted with a plate spindle (40 mm in diameter

and 0.4 mm in gap distance) and the viscosities were recorded under steady-state shear stress from 0.003 Pa to 20 Pa at 23 °C. Raw data were analyzed and extrapolated to obtain the zero-shear viscosity (η_0) under the Newtonian region. Specific viscosity (η_{sp}) was defined as $(\eta_0 - \eta_{solv}) / \eta_{solv}$, where η_{solv} is the solvent viscosity. The surface tension of solutions was measured on a tensiometer (Fisher Scientific Tensiometer 20). Fourier transform infrared spectroscopy (FTIR, Nicolet Nexus 470) was employed to analyze the polymer-solvent-salt interactions within the solutions.

Element analysis (Perkin Elmer 2400 Series II CHNS/O Elemental Analyzer) and energy dispersive spectra (EDS, Oxford Instruments) was employed to confirm the composition of the carbonized Sn/C nanofibers. Scanning electron microscopy (FEI Verios 460L) and field-emission transmission electron microscopy (TEM, Hitachi HF2000) were used to characterize the morphology of the Sn/C nanofibers.

Electrochemical performance was evaluated in lithium-ion half cells. The carbonized nanofibers were ground to powder to form the working electrode by the traditional slurry coating process using a composition of 80 wt% active materials, 10 wt% sodium alginate binder and 10 wt% carbon black. Lithium ribbon (99.9%, Aldrich) was used as the counter electrode, and Celgard 2400 membrane was used as the separator. The electrolyte consisted of a 1 M solution of LiPF_6 dissolved in 1/1 (V/V) ethylene carbonate (EC)/ethyl methyl carbonate (EMC). Coin-type 2032 cells (20 mm diameter, 3.2 mm thickness) were assembled in a high-purity argon-filled glove box. The electrochemical performance was investigated by

galvanostatic charge-discharge experiments at constant current density of 100 mA g⁻¹ with cut-off potentials from 0.01 to 1.50 V (vs. Li/Li⁺) using LAND-CT 2001A battery test system.

3.3 Results and discussion

3.3.1 Solution properties

FTIR was employed to investigate the interactions between PAN, DMF and SnCl₂, and the results are shown in Figure 3.2. The major characteristic peaks of DMF were -C=O stretching (1656.9 cm⁻¹) and OC-N stretching (1389.1 cm⁻¹).^[150] Figure 3.3 (a) shows the interaction between PAN and DMF and formed complex, which can be attributed to the interaction between the electronegative nitrogen of PAN and the electropositive nitrogen of OC-N of DMF. Due to interactions between DMF and PAN, -C=O band shifted from 1656.9 cm⁻¹ to 1666.3 cm⁻¹ while OC-N from 1389.1 cm⁻¹ to 1387.2 cm⁻¹, which was also reported by Phadke and Padhye.^[151, 152] The addition of SnCl₂ into the PAN-DMF solution caused the redshift of -C=O from 1666.3 to 1660.5 cm⁻¹ and blueshift of OC-N from 1387.2 cm⁻¹ to 1389.1 cm⁻¹, which were caused by the formation of the complexes between the electropositive Sn²⁺ and electropositive oxygen in DMF and nitrogen in PAN. Both shifts became smaller with the increasing Sn salt concentration. The formation of PAN-salt complex was due to the interactions between Sn²⁺ and nitrogen in PAN, (Figure 3.3 (b)). DMF-salt interaction was formed because the electropositive nitrogen in DMF tends to interact with negative chloride ion (Figure 3.3 (c)). The results were consistent with that reported by Phadke et al., who added LiCl, ZnCl₂, and AlCl₃ to the PAN-DMF solution.^[151]

The shifted bands are recorded in Table I. The results elucidated the interactions between DMF, PAN and SnCl₂, which had an important impact on the viscosity of precursor solutions and the resultant nanofiber structure.

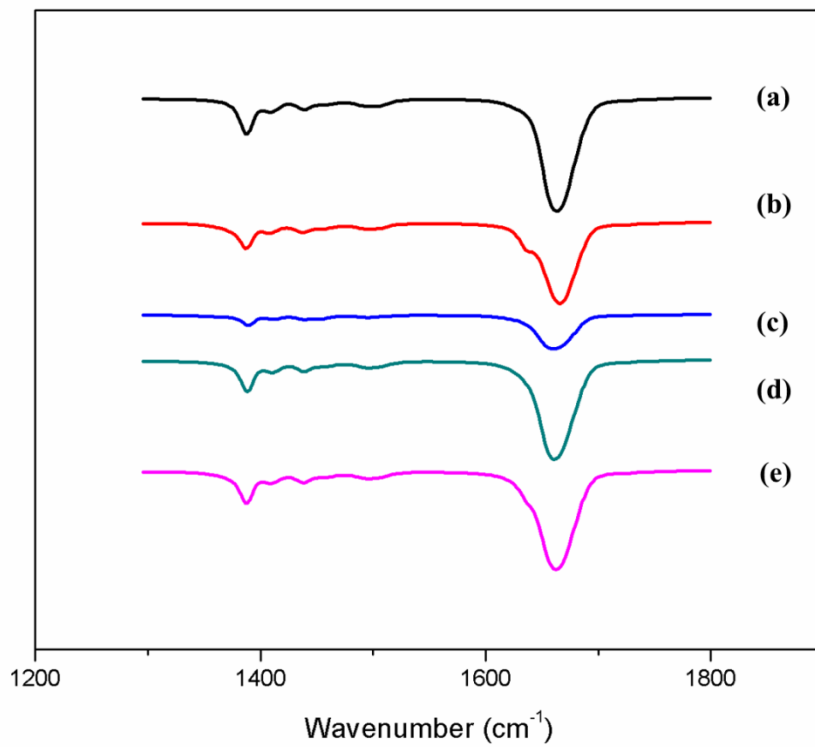


Figure 3.2. FTIR spectra of PAN/DMF with different SnCl₂ concentrations: (a) DMF, (b) 0, (c) 2 wt%, (d) 5 wt%, (e) 8 wt%.

Figure 3.4 shows the effect of salt concentration on the specific viscosity of SnCl₂/PAN solutions. With the addition of Sn salt, the specific viscosity increased significantly due to the interactions between the cation (Sn²⁺) and electronegative oxygen in DMF or nitrogen in PAN, as shown in Figure 3.3. The increase in solution viscosity improves the stability of the newly-formed jets during centrifugal spinning, but may lead to larger fiber diameters.

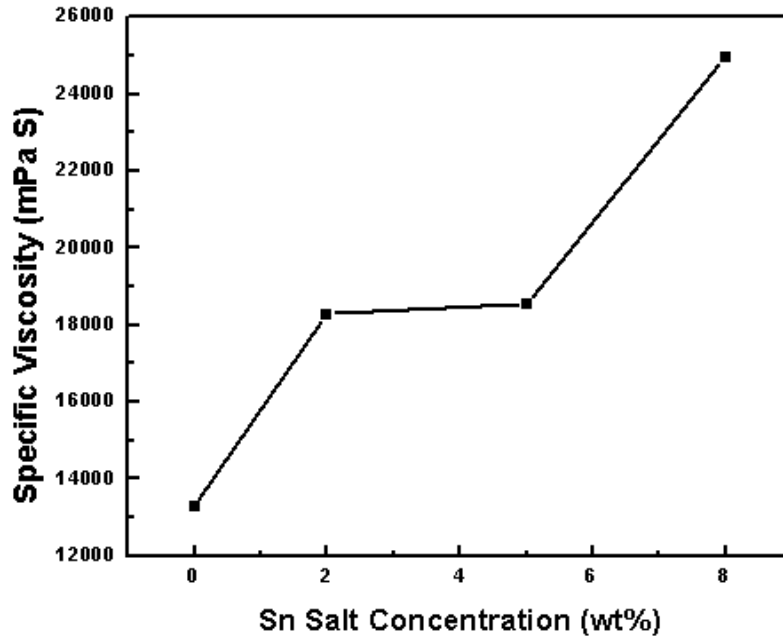


Figure 3.4. Specific viscosity versus Sn salt concentration profile for PAN/DMF solutions.

In addition to viscosity, surface tension also plays a crucial role in fiber formation process. The surface tension is caused by the attractive force between the molecules in the bulk and on the surface of solution.[56] In general, surface tension results in jet instability in the

spinning process.[153] The surface tension measurements unveiled the surface tension change trend with the addition of Sn salt. Figure 3.5 shows the effect of Sn salt on the surface tension of SnCl₂/PAN solutions. The surface tension increased from 41.2 to 54.0, 65.0 and 65.8 when the Sn salt concentration increased from 0 to 2, 5 to 8 wt%.

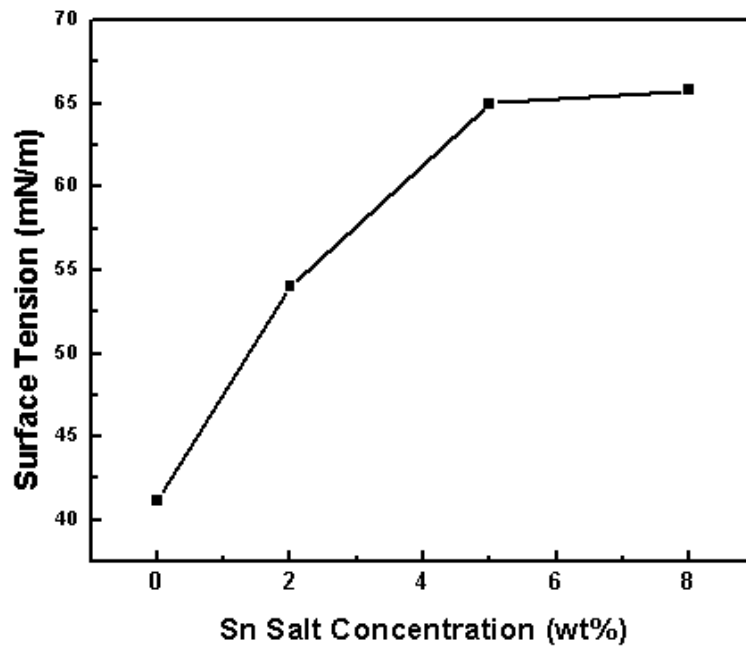


Figure 3.5. Surface tension versus Sn salt concentration profile for PAN/DMF solutions.

3.3.2 Composition and morphology

The element analysis results are shown in Table 3.2. Higher tin amount is observed in 8wt% sample than in 5 and 2wt% Sn/C nanofibers, which is the main reason 8wt% Sn/C nanofibers delivered higher specific capacity in the first cycle.

Table 3.2 Compositions of Sn/C nanofibers prepared by centrifugal spinning

Nanofiber composition	Carbon content (wt%)	Tin content (wt%)
2 wt% Sn@CNFs	57.87	25.4
5 wt% Sn@CNFs	55.40	29.0
8 wt% Sn@CNFs	51.49	33.0

Figure 3.6 shows SEM images of Sn salt/PAN precursor nanofibers with different weight ratios. Smooth surface morphology was observed for the precursor fibers. The average fiber diameters were 420 nm, 429 nm, 1260 nm and 1627 nm, respectively, for samples with Sn salt concentration of 0, 2, 5 and 8wt%. The increasing fiber diameters correspond well with the increasing viscosity shown previously. It is seen in Figure 3.7 that the tin/CNFs exhibit wrinkles and grooves on the nanofiber surface. By randomly analyzing the surface areas with in-situ EDS, element tin was proved to be present in the nanofibers. Fiber diameters ranging from 450 nm to over 1 μm were observed.

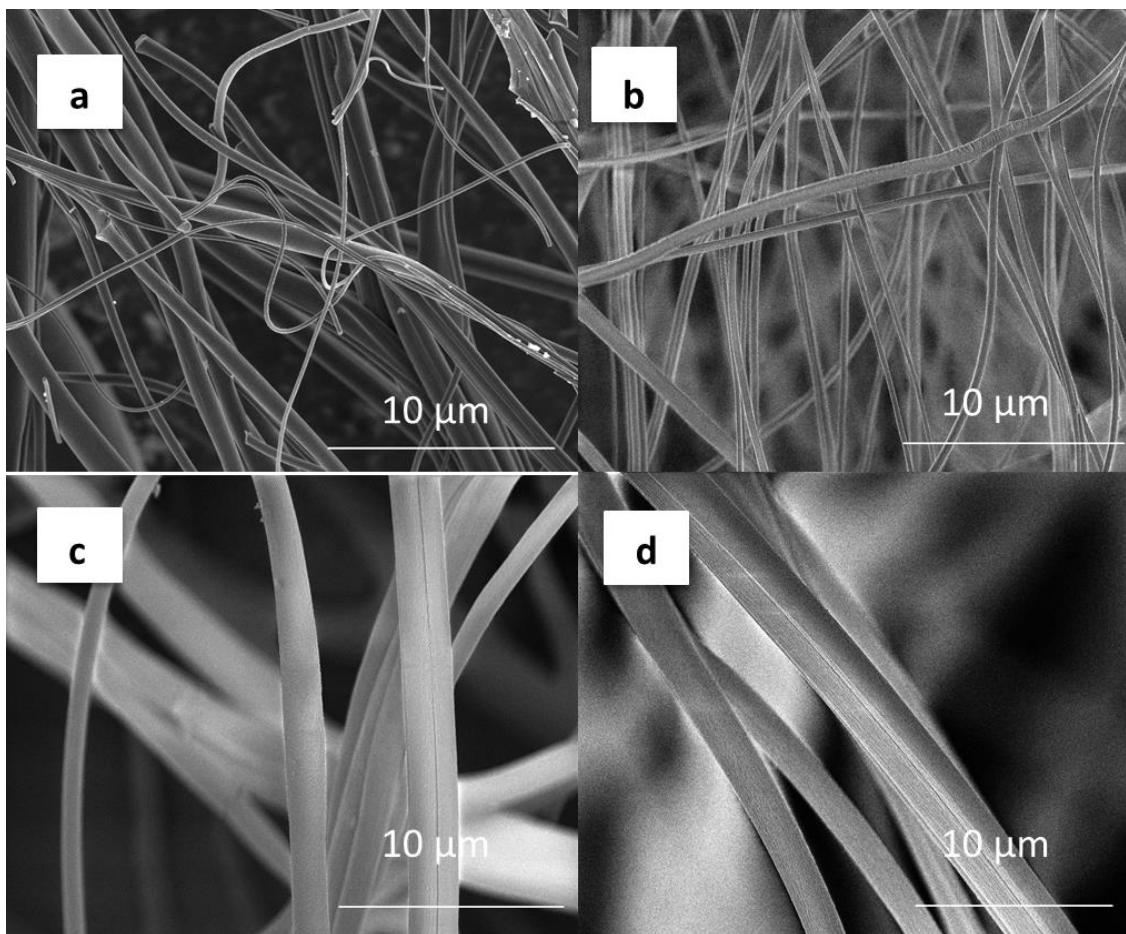


Figure 3.6. SEM images of tin salt/PAN precursor fibers with different weight ratios of PAN/SnCl₂: a)15/0, b) 15/2, c) 15/5, d) 15/8.

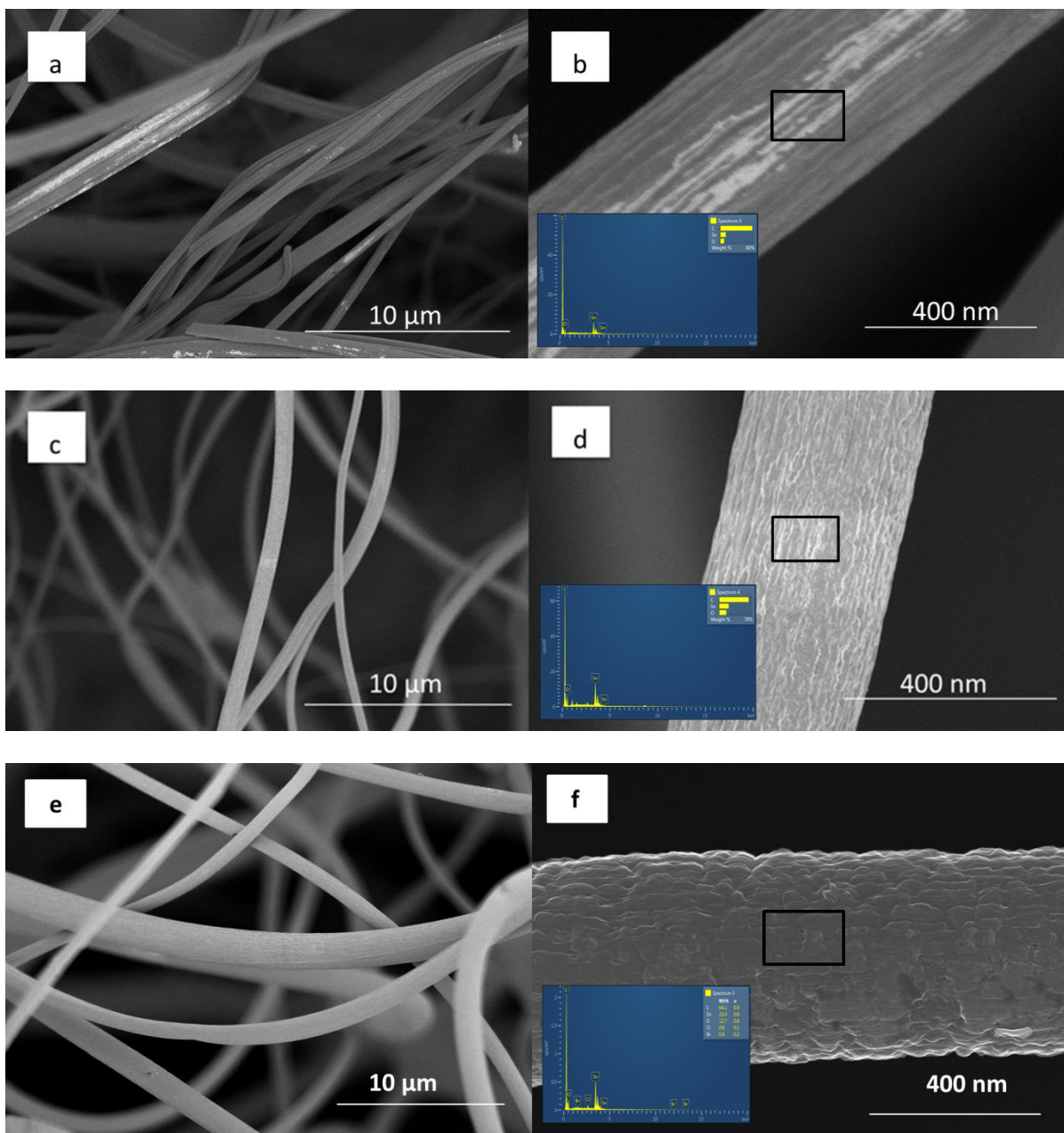


Figure 3.7. SEM images of Sn/C composite nanofibers derived from different weight ratios of PAN/SnCl₂ precursors: a,b) 15/2, c,d) 15/5, e,f) 15/8.

Figure 3.8 exhibits a TEM image of a Sn/C nanofiber prepared from 5 wt% SnCl₂/PAN precursors. Results indicate that Sn nanoparticles are formed and dispersed in the carbon

matrix uniformly, either enwrapped within the fiber or dispersed on the fiber surface. The formation of metallic Sn is caused by the reducing environment created by the carbonization reactions.

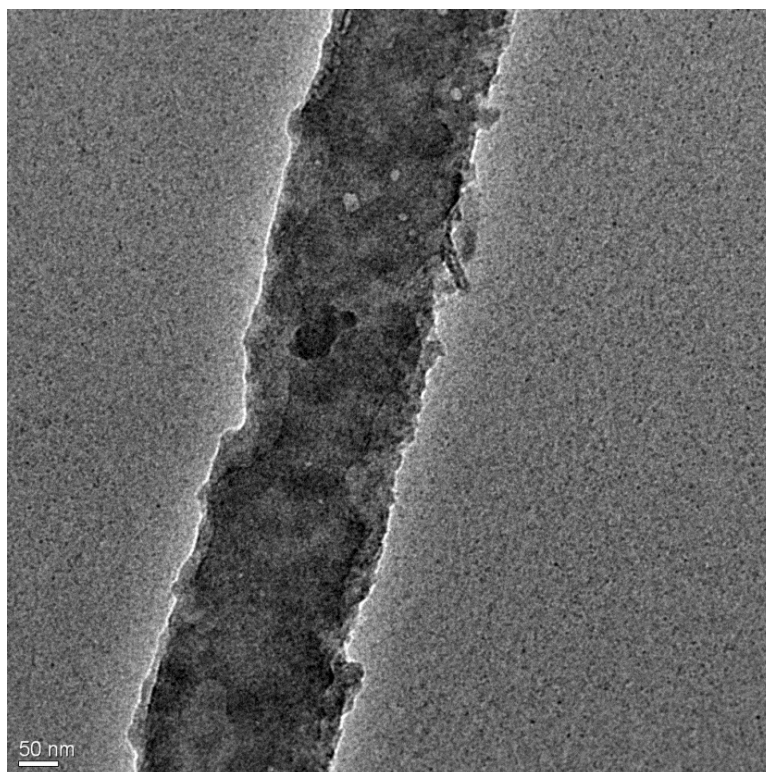


Figure 3.8. TEM image of a Sn/C composite nanofiber derived from 5 wt% SnCl₂/PAN precursor.

3.3.3 Electrochemical performance

Galvanostatic charge-discharge experiments were carried out under a current density of 100 mAg⁻¹ within a voltage window of 0.01-1.5 V to evaluate the electrochemical performance of

Sn/C nanofiber anodes prepared by centrifugal spinning of 0, 2, 5 and 8wt% SnCl₂/15wt% PAN precursors. Figure 3.8 shows the galvanostatic charge-discharge profiles for the second tenth and fifth cycles of the Sn/C nanofibers and corresponding cycling performance. During the initial discharge, solid electrolyte interface (SEI) was formed due to the decomposition of lithium ion-containing electrolyte. SEI is a porous, electronically insulating structure that hinders further electrolyte reduction while acting as a membrane for charge transfer.[124] The voltage plateau below 0.8V is correspond to the alloy-dealloy process between Li and Sn.[143] At the first cycle, the charge capacities were 469, 500, 607 and 535 mAh g⁻¹ for pure CNFs, 2, 5 and 8 wt% of Sn/C nanofibers, respectively. The significant initial capacity loss is partially due to the formation of a SEI layer on the electrode surface during the first discharge.[117] At 50th cycle, the charge capacities were 264, 317, 442 and 327 mAh g⁻¹ for pure CNFs, 2, 5 and 8 wt% of Sn/C nanofibers, respectively.

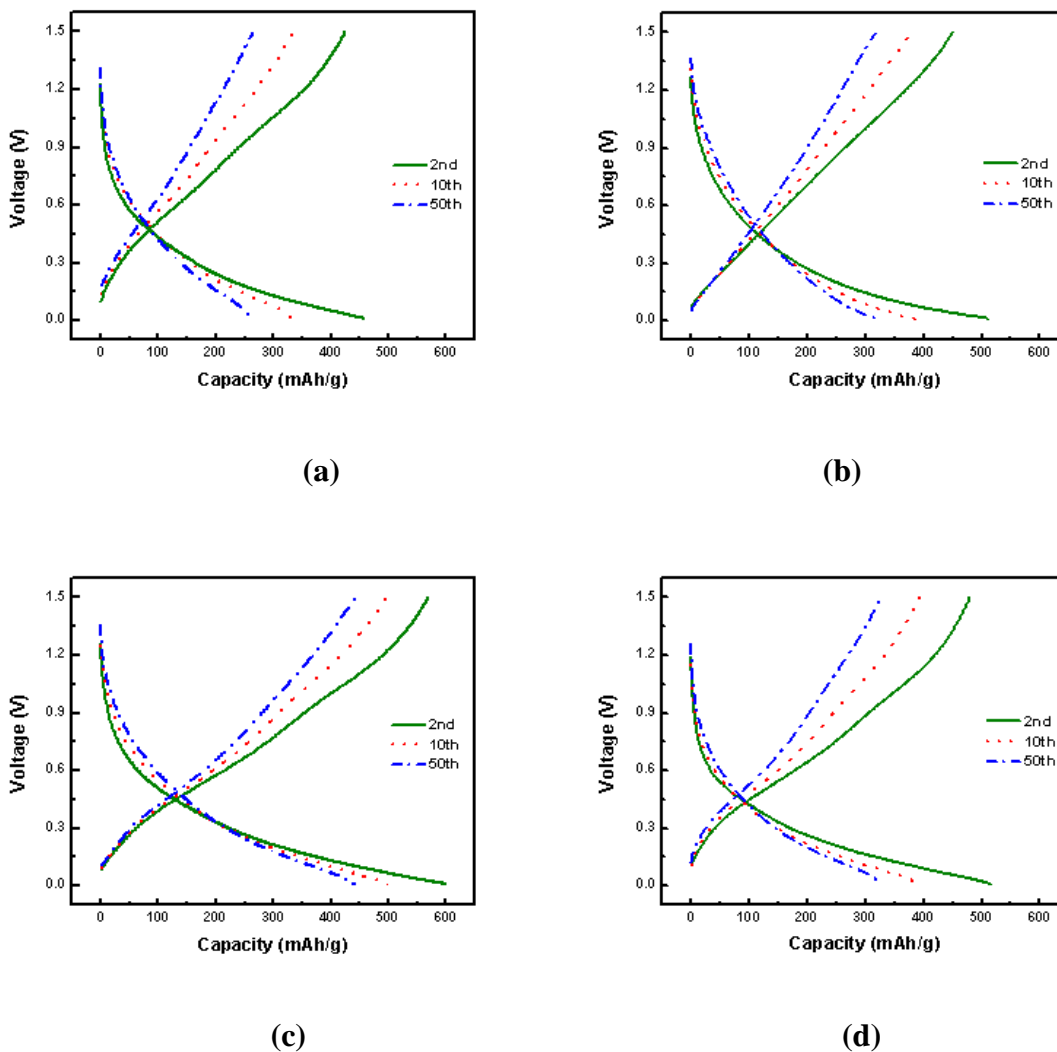


Figure 3.9. Galvanostatic Charge-discharge curves of Sn/C nanofiber anodes derived from: (a) 0 wt%, (b) 2 wt%, (c) 5 wt% and (d) 8wt% SnCl₂/PAN precursors.

Figure 3.10 demonstrates the cycling performance of Sn/C nanofiber anodes derived from 0, 2, 5 and 8 wt% SnCl₂/PAN precursors under a constant current density of 100 mA g⁻¹. After the initial several cycles, the coulombic efficiency of all the four samples approached 100%. At the 50th cycle, the charge capacity were 264 mAh g⁻¹, 317 mAh g⁻¹, 442 mAh g⁻¹ and 327

mAh g⁻¹ for nanofibers anodes derived from 0, 2, 5 and 8 wt% SnCl₂/PAN precursors. Corresponding capacity retentions were 62.11%, 70.44%, 77.54% and 68.27%, respectively. The irreversible capacities of Sn/C nanofiber anodes can be attributed to the first cycle SEI formation and Sn particles aggregations and pulverization during the repeatedly alloying and dealloying processes,[143] while the reversible part are mostly contributed by the Sn nanoparticles enwrapped within the fiber structure and the carbon nanofiber matrix, which can accommodates Sn particle volume expansions during lithiation and delithiation processes.[117, 154]

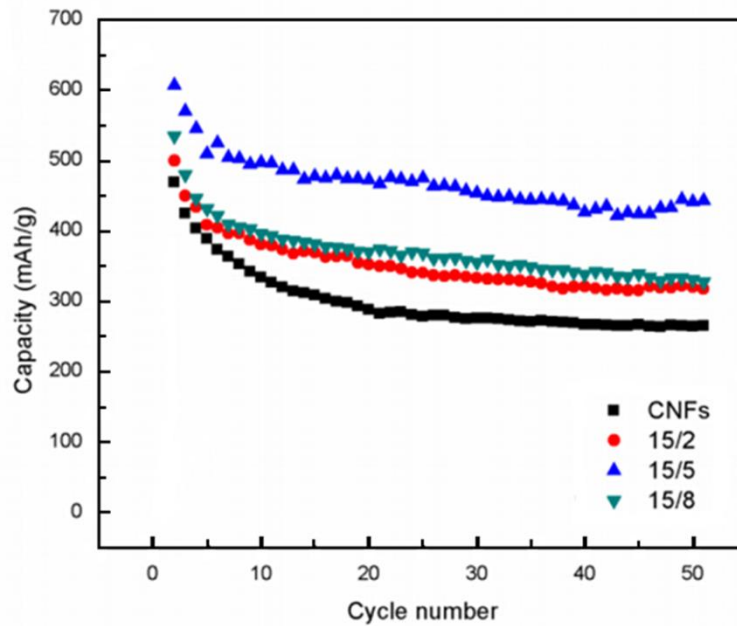


Figure 3.10. Cycling performance of Sn/C nanofiber anodes derived from 0, 2, 5 and 8 wt% SnCl₂/15wt% PAN precursors.

3.4 Conclusion

Sn/C nanofibers were fabricated by centrifugal spinning and subsequent thermal treatment of SnCl₂/PAN precursor solutions. Polymer, solvent and salt interactions were discussed and analyzed, and consequent impacts upon centrifugal spinning were characterized. It was found that the addition of Sn salt increased the specific viscosity of the spinning solution and the diameter of the centrifugally-spun nanofibers. Resultant Sn/C nanofibers were then used as the anode material for lithium-ion batteries. The charge capacity of Sn/C nanofibers prepared from 5 wt% Sn/PAN precursors reached 442 mAh g⁻¹ at 50 the cycle, which is much higher than that of the pre CNFs. In addition, a coulombic efficiency of nearly 100% was achieved for Sn/C nanofibers after the initial cycles, indicating good reversibility. The outstanding electrochemical performance is due to the synergic effects of both CNFs and active Sn particles. Centrifugal spinning is, therefore, verified as an alternative nanofiber fabrication technique to produce nanofiber electrode materials for next-generation lithium-ion batteries.

CHAPTER 4 POROUS CARBON NANOFIBERS PREPARED BY CENTRIFUGAL SPINNING AND THEIR APPLICATION AS ELECTRODE MATERIAL FOR SUPERCAPACITORS

Abstract: So far, CNFs have been mainly produced by electrospinning of precursor fibers and subsequent heat treatment. The low production rate of the electrospinning process hinders the mass production of CNFs and their applications. Recently, much attention has been paid to centrifugal spinning, featured by its high production rate (500 times faster than traditional electrospinning) and simple operation. Herein, centrifugal spinning was utilized to fabricate high-surface area carbon nanofibers from PAN/PMMA polymer blend solutions. In the binary system, PAN served as the carbon precursor while PMMA was decomposed to create the large surface area inside in the fiber. Unique morphologies arose from centrifugal stretching were characterized. These high-surface area CNFs were used as electrode materials in supercapacitors and demonstrated specific capacitance of around 100 F/g.

Keywords: Centrifugal spinning, polymer blend, CNF, supercapacitor.

4.1 Introduction

Supercapacitors are featured by high power density and long cycle life, have attracted enormous interests in recent years and have been used together with high energy density rechargeable batteries in various applications including portables electronics, hybrid electric vehicles and stand-by power systems.[123, 127, 155] Different from typical rechargeable batteries such as lithium-ion batteries, where electrochemical reactions occur by intercalation of Li ions between electrode bulk materials, supercapacitors work by reversibly adsorbing electrolyte ions onto the surfaces of electrode materials.[156] The energy crisis, the development of sustainable energy such as solar, wind energy and the need for electrical propulsion require new developments on novel energy storage technologies.[123] Higher capacitance and longer cycle life are desired for next-generation energy storage systems like supercapacitors. The electrochemical capacitance of supercapacitors is closely associated with the surface area, pore size distribution, and ionic accessibility of the electrode materials.[137] In particular, the high surface is highly desired for supercapacitor electrode materials because it determines the contact area between the electrolyte and electrodes, and consequently the ion transfer pathway and the charge transfer amount contributing to the capacitance.[106, 138, 142, 157-162]

Different from pseudocapacitors, only electrostatic charge adsorption/desorption reactions involve during charge and discharge process in EDLC, which contributes to its large power density. CNFs have been turned out to be a promising material for EDLC electrode material due to their good chemical stability, high conductivity, low resistivity, and high specific

area.[106] Attempts have been made to use electrospinning to produce carbon nanofibers for supercapacitors.[106, 137, 142, 157, 160, 163, 164] However, the low production rate of electrospinning greatly constrains the large-scale production of carbon nanofibers for practical supercapacitor applications.

Recently, centrifugal spinning, an alternative nanofiber fabrication method to electrospinning, has aroused enormous interests among researchers due to its high production rate and ease of operation.[47-51, 62] CNFs can be made through subsequent thermal treatment of centrifugally-spun polymer precursors. In this work, we utilized centrifugal spinning to prepare PAN/PMMA inlands-in-the-sea nanofibers, where PAN is the island phase and PMMA is the sea. These centrifugally-spun precursors were thermally treated to form high-surface area CNFs, during which PAN was converted to carbon while PMMA was decomposed to create the large surface area. Figure 4.1 illustrates the fabrication process of high-surface area carbon nanofibers by centrifugal spinning of PAN/PMMA polymer blend solutions. The effect of PAN/PMMA weight ratios on the nanofiber morphology was analyzed. Resultant nanofibers were used as electrode materials for EDLCs and demonstrated a specific capacitance of around 100 F/g.

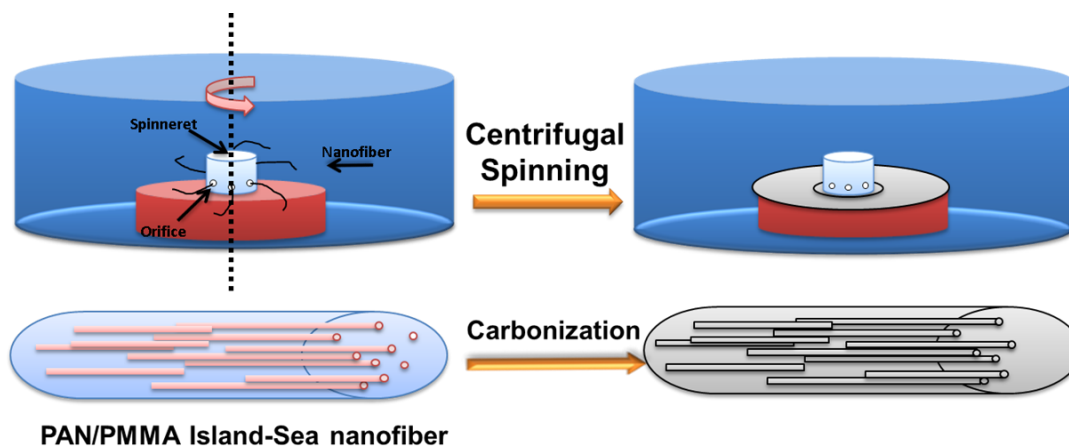


Figure 4.1. Schematic of the preparation of porous carbon nanofibers by centrifugal spinning of PAN/PMMA blend.

4.2 Experimental

4.2.1 Materials and preparation of carbon nanofibers

Polyacrylonitrile (PAN, Pfaltz & Bauer Inc., $150,000 \text{ g mol}^{-1}$), polymethylmethacrylate (PMMA, Aldrich, $350,000 \text{ g mol}^{-1}$) and N,N-dimethylformamide (DMF, Aldrich) were used as purchased.

PAN and PMMA were dissolved in DMF, and mechanically stirred for 24 hours at $90 \text{ }^\circ\text{C}$, to obtain blend solutions for centrifugal spinning. In these solutions, the PAN/PMMA weight ratios were 10/90, 20/80, 30/70, 50/50 and 100/0 while keeping the polymer concentration constant (16 wt%).

PAN/PMMA islands-in-the-sea nanofibers were produced by centrifugal spinning with a rotating speed of 3500 rpm. The spinneret had a cylindrical shape with 2 cm in height, 1.5 cm

in radius and a nozzle diameter of 0.4 mm. Resultant nanofibers were stabilized in air environment at 280 °C for 5.5 h with a heating rate of 5 °C min⁻¹ and then carbonized at 700 °C and 800 °C, respectively, for 2 h in argon with a heating rate of 2 °C min⁻¹, during which PAN was pyrolyzed to carbon and PMMA was decomposed to create large surface area.

4.2.2 Solution property and fiber structure characterizations

Viscosities of the centrifugal spinning solutions were measured to evaluate the spinnerability. During the viscosity measurements, pure DMF and PAN/PMMA blend solutions were loaded into a viscometer (ATS Rheosystem) fitted with a plate spindle (40mm in diameter and 0.4 mm in gap distance) and the viscosities were recorded under steady-state shear stress from 0.003 Pa to 40 Pa at 23 °C. Raw data were analyzed to obtain the zero-shear viscosity (η_0) under the Newtonian region. Solution specific viscosity (η_{sp}) was defined as $(\eta_0 - \eta_{solv})/\eta_{solv}$, where η_{solv} is the solvent viscosity.[51]

The Brunauer-Emmett-Teller (BET) measurements (Gemini VII 2390a Micromeritics Analyzer and Smartprep 065 Degassing Unit) were utilized to calculate the specific surface areas of the porous CNFs. It should be noted that the BET surface area does not directly correspond to the reaction interface between electrolyte and electrode, but it is still a good estimation of the potential reaction sites. Samples were first loaded into a 300 °C degassing unit with flowing nitrogen gas in order to remove contaminants on the surfaces and were then

loaded into the BET testing system. Scanning electron microscopy (FEI Verios 460L) was employed to analyze the surface morphology of nanofibers before and after thermal treatment.

4.2.3 Electrochemical measurements

Nanofiber electrodes were prepared by mixing 70 wt% active materials, 20 wt% carbon black, and 10 wt% polyvinylidene difluoride (PVDF) binder dispersed in N-methyl-2-pyrrolidone (NMP). The mixed slurry was then applied onto a stainless steel mesh, which served as a current collector. Two-electrode supercapacitors were assembled with two identical electrodes mounted in a Swagelok-type cell. The two electrodes were separated by a glass microfiber paper (WhatmanTM) and the electrolyte was 6 M KOH aqueous solution. Cyclic voltammetry was carried out under a scan rate of 10 mV/s and a voltage window from 0.01v to 1v. Nyquist plots were obtained for the cells in the frequency range from 100 kHz to 100 mHz at an open circuit voltage of 5 mV.

4.3 Results and discussion

4.3.1 Structure Characterization

Viscosity plays a major role in determining the spinnerability and final morphology of centrifugally-spun nanofibers. Our previous work [48] has demonstrated the existence of a critical concentration, which indicates the threshold concentration beyond which sufficient polymer entanglements can be formed to produce uniform, bead-free nanofibers. Figure 4.2 shows the effect of PAN/PMMA weight ratios on the specific viscosity of PAN/PMMA solutions. It was found that with the decrease in the PMMA content, the specific viscosity

deceases, and it is understandable because the majority phase PMMA has a higher molecular weight, indicating more polymer chain entanglements, the greater drag force induced from viscous PMMA increased the solution viscosity.

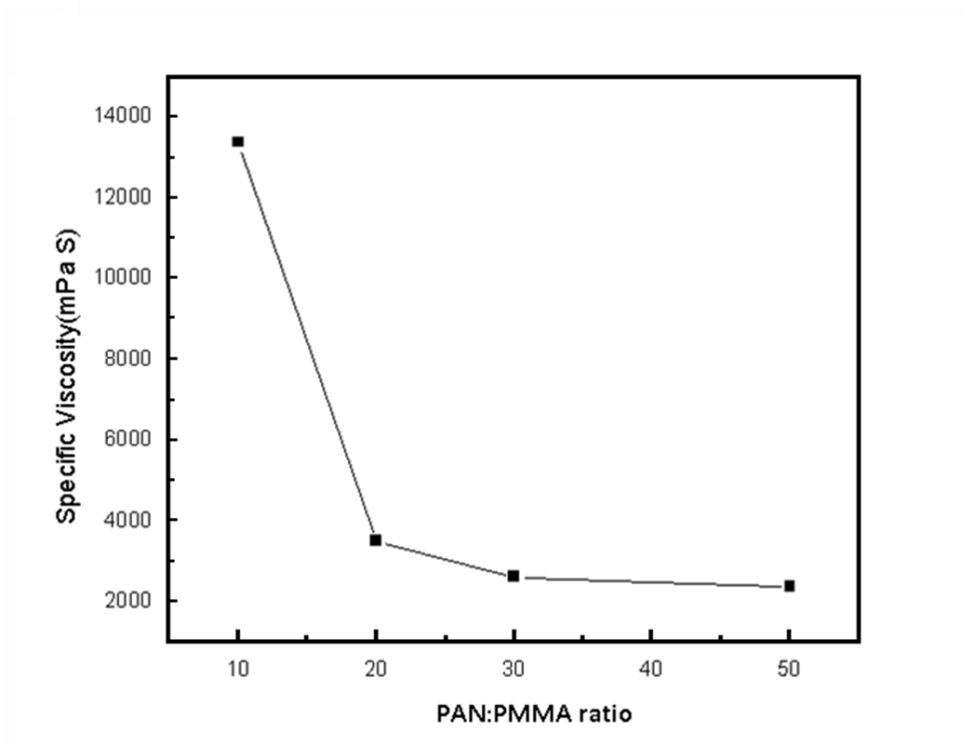


Figure 4.2. Specific viscosity versus PAN/PMMA weight ratios.

Figure 4.3 shows SEM images of centrifugally-spun PAN/PMMA nanofibers before thermal treatment. The average fiber diameters were 4.55, 3.08, 4.03 and 3.63 μm respectively, with PAN/PMMA weight ratios of 1:9, 2:8, 3:7 and 5:5. Grooves were observed on the

centrifugally-spun nanofiber surfaces, probably due to the phase separation within polymer blends and the large stretching force exert upon them during the centrifugal spinning.

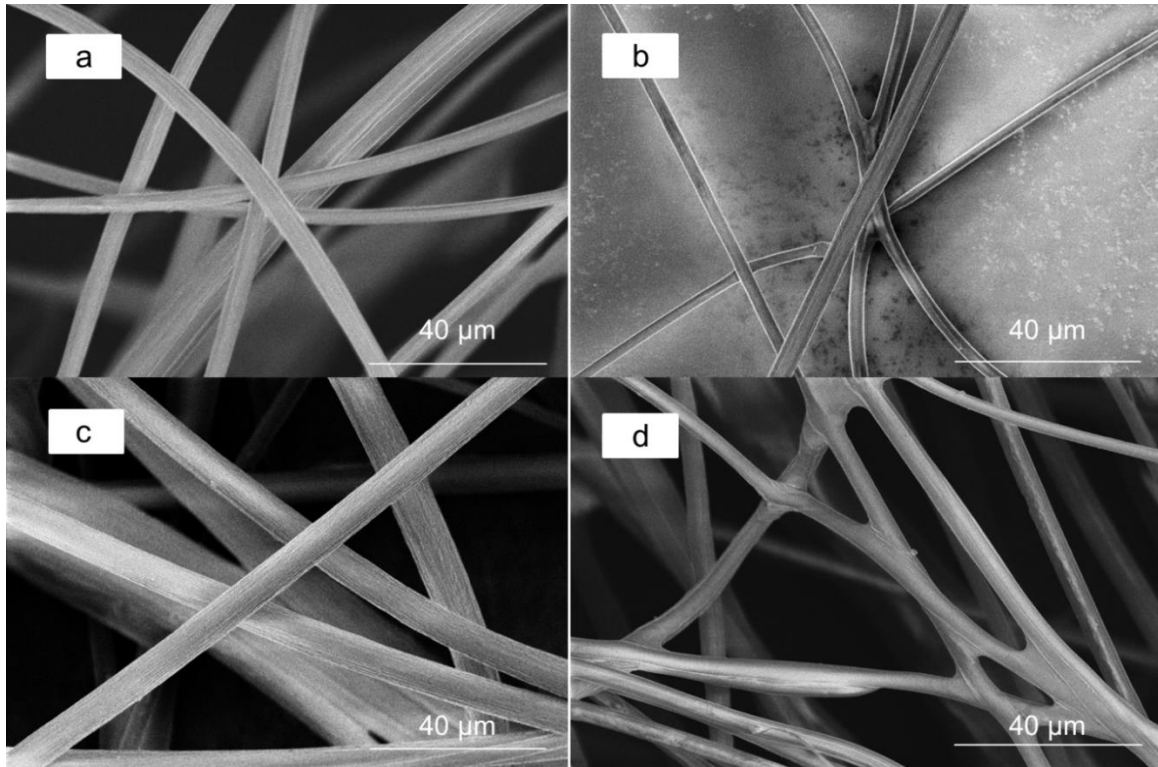
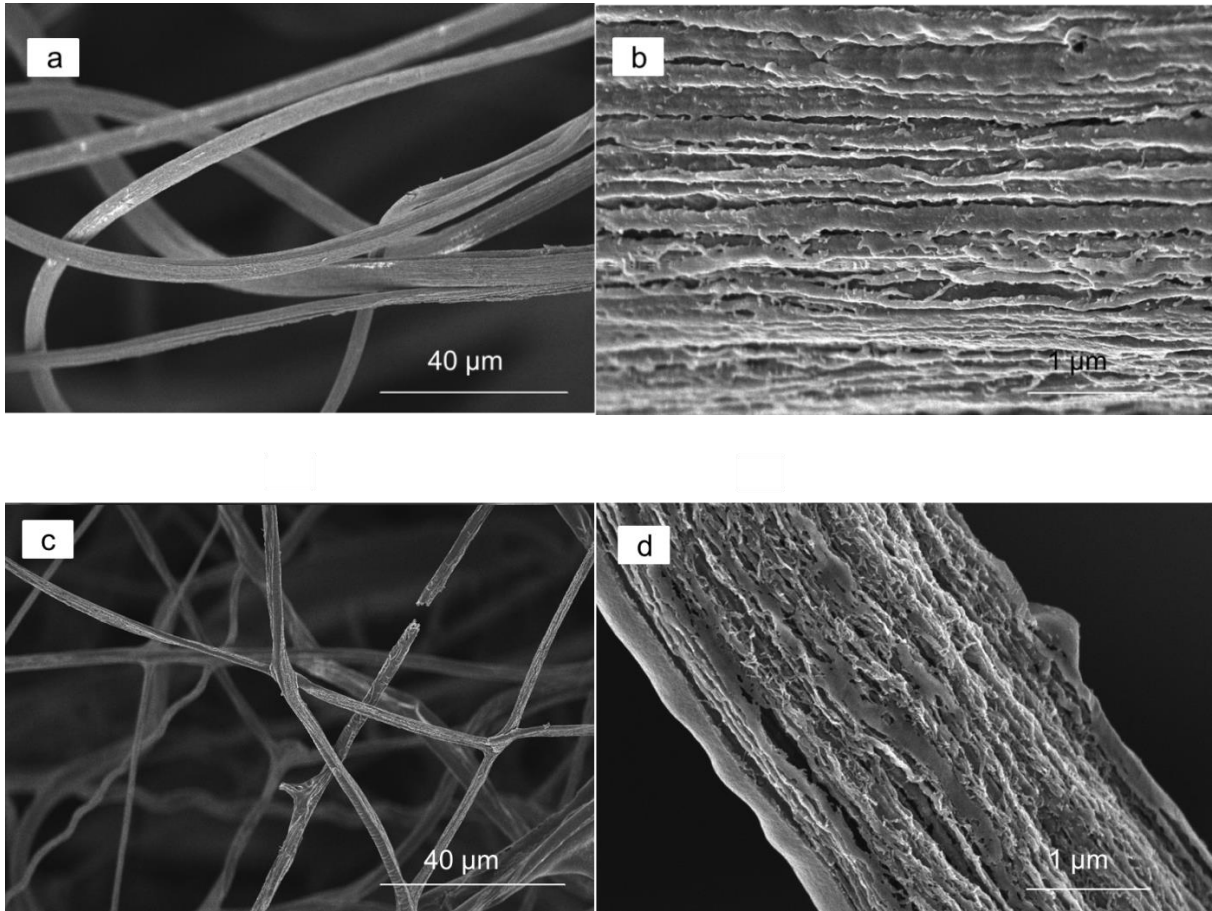


Figure 4.3. Centrifugally-spun PAN/PMMA nanofibers with different PAN/PMMA weight ratios: a) 1:9, b) 2:8, c) 3:7, d) 5:5.

Figure 4.4 shows SEM images of CNFs prepared by thermally treating centrifugally-spun PAN/PMMA precursors at 800 °C. The nanofibers showed longitudinally aligned fibril structures after the decomposition of PMMA, which was induced by phase separation between PAN/PMMA and large stretching due to centrifugal force. The diameters of the fibrils ranged from 30 nm to 170 nm for 1:9, 2:8 and 3:7 PAN/PMMA precursor samples.

Both PAN/PMMA (2:8) and PAN/PMMA (3:7) nanofibers showed similar fibril structures with fibril diameters ranging from 25 nm to 50 nm. However, PAN/PMMA (5:5) nanofibers did not show clear fibril structure, Instead, they presented deep grooves and wrinkles on the fiber surface with a width of around 220 nm.



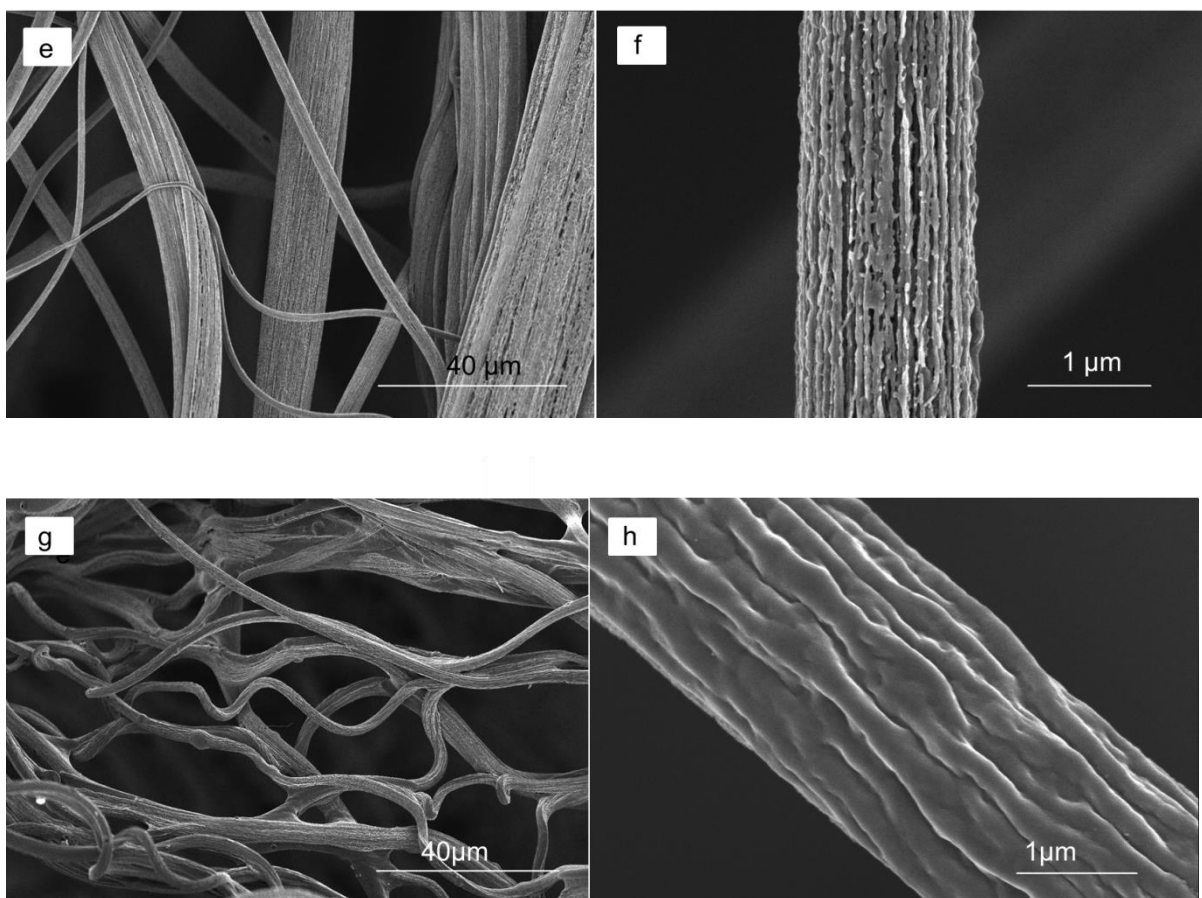


Figure 4.4. SEM images of carbon nanofibers thermally-treated from centrifugally-spun PAN/PMMA precursors with different weight ratios: (a,b) 1:9, (c,d) 2:8, (e,f) 3:7, (g,h) 5:5.

Surface area and pore structural properties were characterized by BET and summarized in Table 4.1. CNFs prepared from PAN/PMMA precursor fibers with a weight ratio of 2:8 treated at 800 °C reached $420.05 \text{ m}^2 \text{ g}^{-1}$, which is similar to that of PAN-based porous carbon nanofiber webs activated by ZnCl_2 . [165] The results were consistent with the SEM observations, for CNFs prepared from PAN/PMMA weight ratios of 2:8 and 3:7 at 800 °C possessed finer fibrous structures and presented higher surface areas. Pore sizes for all

samples were consistent, which were all around 4.1 nm. To make a comparison, CNFs prepared from PAN/PMMA precursor fibers with a weight ratio of 3:7 at 700 °C only reached a surface area of 147.32 m² g⁻¹ and a total pore volume of 0.101 cm³ g⁻¹, while their 800 °C counterparts reached a surface area of 316.38 m² g⁻¹ and a total pore volume of 0.134 cm³ g⁻¹. The results demonstrated the importance of carbonization temperature upon the final morphology and physical properties of CNFs prepared by centrifugal spinning.

Table 4.1 Physicochemical characterizations of CNFs thermally-treated from PAN/PMMA precursors with different weight ratios at 800 °C

	1:9	2:8	3:7	5:5	10:0
BET surface area (m ² g ⁻¹)	224.20	420.05	316.38	240.02	133.59
Average pore size (nm)	4.130	4.131	4.129	4.129	4.129
Pore volume (cm ³ g ⁻¹)	0.155	0.146	0.134	0.088	0.092

4.3.2 Electrochemical characterization

The electrochemical properties of CNFs thermally-treated from PAN/PMMA precursor fibers with a weight ratio of 3:7 at 700 °C and 800 °C were tested to verify the importance of surface area and at the same time, demonstrate the feasibility of using CNFs prepared by centrifugal spinning as electrode materials for supercapacitors. The cyclic voltammetry (CV) profiles at different scan rates are shown in Figure 4.5. The CV patterns are distorted rectangular without the presence of faradaic peaks, indicating typical EDLC behavior.[137, 160] According to the CV curves, the specific capacitance of the electrodes was calculated via equation 4.1.

$$C_s = 2(\int IdV)/(vm\Delta V) \quad (4.1)$$

where I is the current in a given potential (A), V the potential (V), v is the potential scan rate (V/s), m the mass of the electrode (g), and ΔV the potential difference (V).[160, 166] For CNFs treated at 700 °C, with the scan rate increasing from 5 to 100 mV/s, the specific capacitance fell from 91 to 50 F/g while for the CNFs treated at 800 °C, the specific capacitance decreased from 102 to 77 F/g, showing improved rate performance. Since CNFs treated at 700 °C only possesses a BET surface area of 147.32 m² g⁻¹ and a total pore volume of 0.101 cm³ g⁻¹, while their 800 °C counterparts exhibit a surface area of 316.38 m² g⁻¹ and a total volume of 0.134 cm³ g⁻¹. The results can be attributed to factors such as decreased transport pathway length for ions such as K⁺ and OH⁻ in aqueous electrolyte, higher specific reaction areas, and lower contact resistance between the electrode-electrolyte interfaces, which was later verified in EIS.[124, 137]

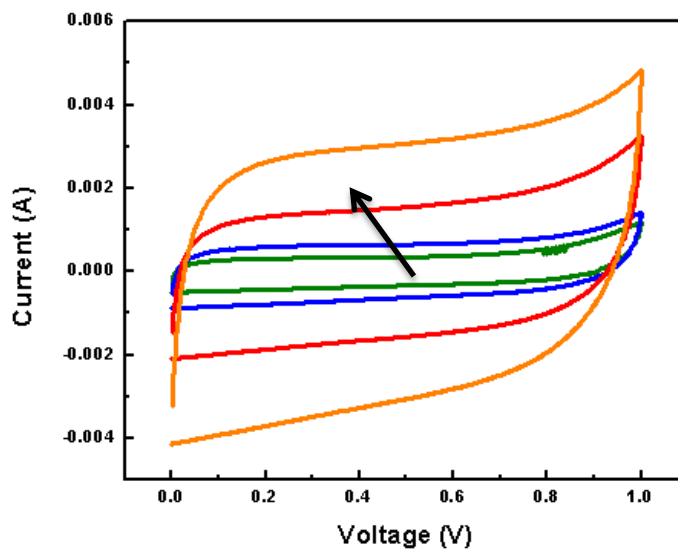
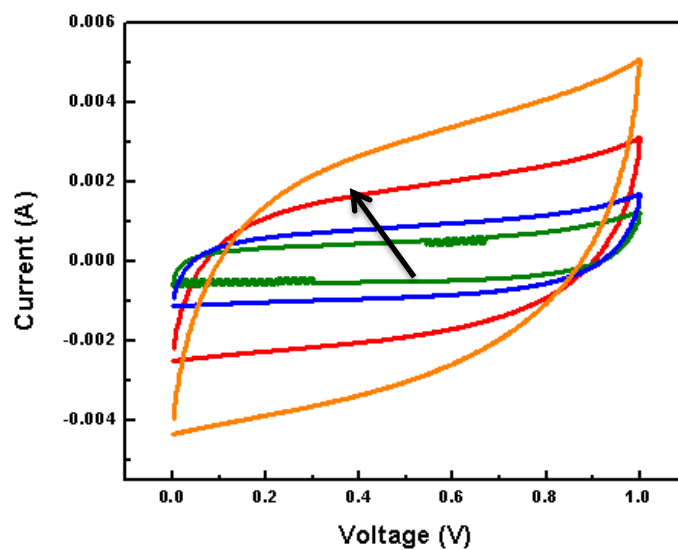


Figure 4.5. CV curves of carbon nanofibers with 3:7 PAN/PMMA weight ratio, and thermally-treated at: (a) 700 °C and (b) 800 °C. Arrows indicate the increasing scan rate from 10 to 100 mV s^{-1} .

The electrochemical impedance spectra (EIS) were measured to study the impedance of CNFs prepared by centrifugal spinning (Figure 4.6). The frequency range used was from 100 KHz to 100 MHz. Both Nyquist plots showed a single semicircle in the high frequency region and a sloped line in the low frequency region. The ideal capacitance gives rise to a straight line along the imaginary axis, while in a real capacitor this line has a finite slope that represents the diffusive resistivity of the electrolyte within the micro-/mesopores of the electrode.[159] It is seen from Figure 4.6 that CNFs treated at 800 °C exhibited a smaller semicircle arc (4.12 Ω) in the high frequency region than the 700 °C treated counterpart (10.0 Ω), and a more vertical line in lower frequency region than those treated at 700 °C, indicating smaller charge transfer resistance [141, 160, 167] and lower impedance on the electrode/electrolyte interface, which corresponded well with BET surface area and pore volume characterization results.[168]

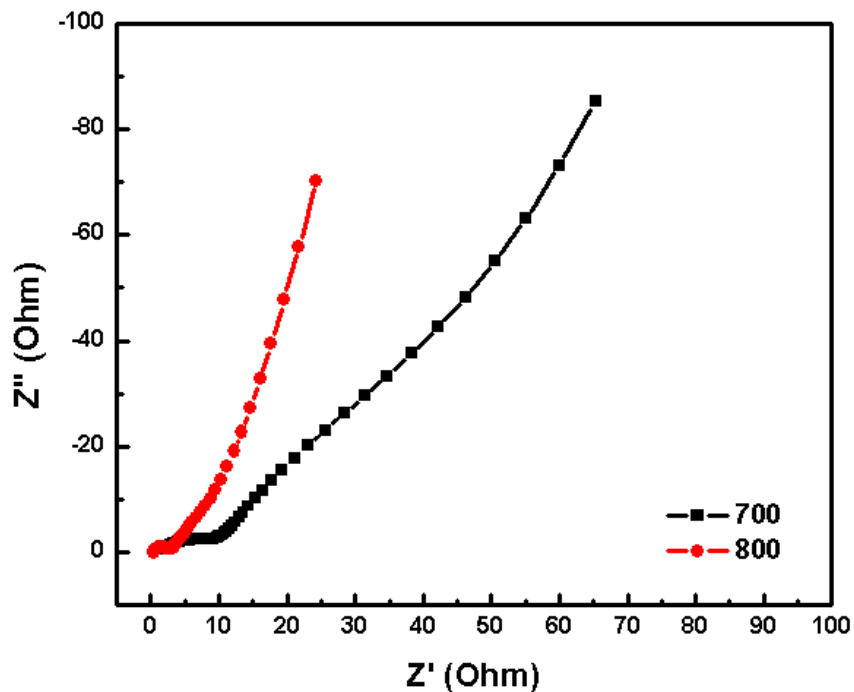


Figure 4.6. Nyquist plots for carbon nanofibers prepared from PAN/PMMA precursor fibers with a weight ratio of 3:7 at 700 °C, 800 °C. The impedance was tested at an open circuit voltage of 5 mV.

4.4 Conclusion

Centrifugally-spun PAN/PMMA islands-in-the-sea nanofibers were fabricated and were thermally-treated to form high-surface area CNFs for use as electrode materials in supercapacitors. The supercapacitor performance of the resultant CNFs was comparable to that of electrospun counterparts. Results demonstrated that CNF treated at 800 °C had superior performance than those treated at 700 °C, probably due to better synergic effects of BET surface area, pore size distribution and pore volume, all of which affect the ion-charge

transfer and effective adsorption upon electrode-electrolyte interface. Centrifugal spinning is, therefore, verified as an alternative nanofiber fabrication technique to produce nanofiber electrode materials for next-generation supercapacitors.

CHAPTER 5 CONCLUSIONS

The world energy crisis and the development of new sustainable energy are pushing the limits in the area of energy storage and conversion systems. Over decades of research and development, carbonaceous materials, from graphite, carbon nanotubes to carbon nanofibers, have become the most studied energy storage materials. Carbon nanofibers, featured by large specific area, ideal electrical and mechanical properties, have been used in both lithium-ion batteries and supercapacitors. Currently, most carbon nanofibers are produced by electrospinning of precursor fibers with subsequent heat treatment. However, the low production rate and high cost of electrospinning hinder the practical application of carbon nanofibers as a useful energy storage material.

Recently, centrifugal spinning, a high-rate and low-cost nanofiber production technique, has experienced great progress and attracted much attention. Various polymeric and ceramic micro-/nanofibers have been fabricated by using this technique. Nonetheless, no work has been done to explore the feasibility of using CNFs prepared by centrifugal spinning for energy storage applications.

In Chapter 3, Sn/C composite nanofibers were prepared by centrifugal spinning and subsequent carbonization process with 0, 2, 5, and 8 wt% SnCl₂(II) chloride/PAN precursors. Interactions between salt, polymer chain and solvent molecules were investigated to guide the production of carbon nanofibers, and the composite nanofibers were then used as anodes

in lithium-ion batteries. Results showed that Sn/C nanofiber anodes prepared from 5 wt% SnCl₂/PAN precursor delivered the highest specific capacity (442 mAh g⁻¹) after 50 cycles and a coulombic efficiency over 99%.

In Chapter 4, PAN and PMMA were employed to produce phase separation polymer blend solutions. Centrifugally-spun nanofibers with different PAN/PMMA weight ratios were prepared and characterized. It was found that CNFs prepared from PAN/PMMA precursor fibers with weight ratios of 3:7 and 2:8 exhibited larger surface area compare to other CNFs. PAN/PMMA precursor fibers with a weight ratio of 3:7 were also treated at 700 °C and 800 °C, respectively, to investigate the effects of carbonization upon morphology and electrochemical performance. It has been demonstrated that the CNFs prepared from precursor fibers with a PAN/PMMA weight ratio of 3:7 at 800 °C delivered the highest specific capacitance of 102 F/g, and a 75.5% of capacitance retention rate under a scan rate as high as 100 mV/s.

CHAPTER 6 RECOMMENDATION WORK

Results described in Chapter 3 and Chapter 4 demonstrate the feasibility of using centrifugal spinning as an alternative approach to produce functional energy-storage nanofibers, which can be utilized for lithium-ion batteries and supercapacitors. The focus of future work should be on the fundamental understanding of the centrifugal spinning process, and the utilization of such first-principle knowledge to manipulate structures and properties of the resultant centrifugally-spun nanofibers. The recommended future work includes but not limited to:

6.1 High speed camera observation upon fiber formation process during centrifugal spinning

A closer observation and investigation of the nanofiber formation process during centrifugal spinning is crucial in the early development stage for this technique. Just like electrospinning, solution jet in different spinning stages may experience different force changes and geometrical distortions, characteristic shape like Taylor cone observed in electrospinning may also be formed. The observation research shall guide future centrifugal spinning equipment design and optimize fiber production procedures for various applications including energy storage.

6.2 Centrifugally-spun core-shell silicon-enwrapped nanofibers for use as anode in lithium-ion batteries

Silicon is a promising anode material for lithium-ion batteries due to its high specific capacity. However, its application is hindered by severe volume expansion and pulverization

during reversible intercalation of lithium within silicon. Silica is usually used as sacrificial content in the structure design for silicon anode materials. In our design, core-shell silicon-enwrapped nanofibers will be produced by co-axial centrifugal spinning by using tetraethyl orthosilicate and silicon as core solution and PAN as shell solution. Specific designed co-axial spinneret will be used in the experiment. Silica will be etched away during post treatment, leaving empty spaces in the core, which can accommodate the volume expansion originated from silicon. Easy to scale-up, high specific capacity anode materials thus can be expected to be fabricated based on using centrifugal spinning.

6.3 Centrifugally-spun nanofibers for use as electrode for pseudocapacitors

EDLC symmetric capacitors have limited energy density due to the nature of electrostatic charge adsorption. Different from EDLC, pseudocapacitor materials are based on metal oxides or conducting polymers, involving faradic redox reactions, and thus contribute much higher specific capacitance compare to EDLC. Experimental approaches include but not limited to: fabricating centrifugally-spun electric conductive polymers such as polyaniline and polypyrrole, combining centrifugally-spun porous carbon with metal oxide like RuO_2 , IrO_2 and MnO_2 , and creating CNT-contained centrifugally-spun carbon nanofibers, all of which can serve as potential candidates for supercapacitor electrode materials.

REFERENCES

1. Al-Saleh, M.H. and U. Sundararaj, *A review of vapor grown carbon nanofiber/polymer conductive composites*. Carbon, 2009. **47**(1): p. 2-22.
2. Ji, L. and X. Zhang, *Fabrication of porous carbon nanofibers and their application as anode materials for rechargeable lithium-ion batteries*. Nanotechnology, 2009. **20**(15): p. 155705.
3. Zuo, F., et al., *Nanofibers from Melt Blown Fiber-in-Fiber Polymer Blends*. ACS Macro Letters, 2013. **2**(4): p. 301-305.
4. Kim, C., et al., *Synthesis and characterization of porous carbon nanofibers with hollow cores through the thermal treatment of electrospun copolymeric nanofiber webs*. Small, 2007. **3**(1): p. 91-95.
5. Che, G., et al., *Chemical vapor deposition based synthesis of carbon nanotubes and nanofibers using a template method*. Chemistry of Materials, 1998. **10**(1): p. 260-267.
6. Gopal, R., et al., *Electrospun nanofibrous filtration membrane*. Journal of Membrane Science, 2006. **281**(1-2): p. 581-586.
7. Li, W.-J., et al., *Electrospun nanofibrous structure: A novel scaffold for tissue engineering*. Journal of Biomedical Materials Research, 2002. **60**(4): p. 613-621.
8. Zeng, J., et al., *Biodegradable electrospun fibers for drug delivery*. Journal of Controlled Release, 2003. **92**(3): p. 227-231.
9. Ding, B., et al., *Electrospun nanomaterials for ultrasensitive sensors*. Materials Today, 2010. **13**(11): p. 16-27.

10. Formo, E., et al., *Functionalization of electrospun TiO₂ nanofibers with Pt nanoparticles and nanowires for catalytic applications*. Nano Letters, 2008. **8**(2): p. 668-672.
11. Yanilmaz, M., et al., *Nanoparticle-on-Nanofiber Hybrid Membrane Separators for Lithium-ion Batteries via Combining Electrospraying and Electrospinning Techniques*. Journal of Membrane Science, 2014.
12. Xia, X., et al., *The effects of electrospinning parameters on coaxial Sn/C nanofibers: Morphology and lithium storage performance*. Electrochimica Acta, 2014.
13. Li, S., et al., *Comparison of Si/C, Ge/C and Sn/C composite nanofiber anodes used in advanced lithium-ion batteries*. Solid State Ionics, 2014. **254**: p. 17-26.
14. Xue, L., et al., *A simple method to encapsulate SnSb nanoparticles into hollow carbon nanofibers with superior lithium-ion storage capability*. Journal of Materials Chemistry A, 2013. **1**(44): p. 13807.
15. Li, Y., et al., *Structure control and performance improvement of carbon nanofibers containing a dispersion of silicon nanoparticles for energy storage*. Carbon, 2013. **51**: p. 185-194.
16. Fu, K., et al., *Aligned carbon nanotube-silicon sheets: a novel nano-architecture for flexible lithium ion battery electrodes*. Adv Mater, 2013. **25**(36): p. 5109-14.
17. Wu, J., et al., *Electrospinning of multilevel structured functional micro-/nanofibers and their applications*. Journal of Materials Chemistry A, 2013. **1**(25): p. 7290-7305.
18. Raghavan, P., et al., *Electrospun polymer nanofibers: The booming cutting edge technology*. Reactive and Functional Polymers, 2012. **72**(12): p. 915-930.

19. Bailey, A.G., *Electrostatic spraying of liquids*. 1988: Research Studies Press Somerset, England.
20. Formalas, A., *US patent, 1 975 504, 1934;(b) J. Doshi and DH Reneker*. *J. Electrostat*, 1995. **35**: p. 151.
21. Reneker, D.H. and I. Chun, *Nanometre diameter fibres of polymer, produced by electrospinning*. *Nanotechnology*, 1996. **7**(3): p. 216.
22. Yarin, A., S. Koombhongse, and D. Reneker, *Bending instability in electrospinning of nanofibers*. *Journal of Applied Physics*, 2001. **89**(5): p. 3018-3026.
23. Frenot, A. and I.S. Chronakis, *Polymer nanofibers assembled by electrospinning*. *Current opinion in colloid & interface science*, 2003. **8**(1): p. 64-75.
24. Demir, M.M., et al., *Electrospinning of polyurethane fibers*. *Polymer*, 2002. **43**(11): p. 3303-3309.
25. Choi, J., et al., *High surface area mesoporous titanium–zirconium oxide nanofibrous web: a heavy metal ion adsorbent*. *Journal of Materials Chemistry A*, 2013. **1**(19): p. 5847-5853.
26. Dan Li, Y.X., *Electrospinning of nanofibers: reinventing the wheel?* . *Adv Mater*, 2004. **16**(14).
27. Kim, J.S. and D.H. Reneker, *Polybenzimidazole nanofiber produced by electrospinning*. *Polymer Engineering & Science*, 1999. **39**(5): p. 849-854.
28. Zhang, X., *Fundamentals of Fiber Science*. 2014: DEStech Publications, Inc.

29. Choi, J., et al., *High surface area mesoporous titanium–zirconium oxide nanofibrous web: a heavy metal ion adsorbent*. Journal of Materials Chemistry A, 2013. **1**(19): p. 5847.
30. Qin, X.H., et al., *Effect of different salts on electrospinning of polyacrylonitrile (PAN) polymer solution*. Journal of applied polymer science, 2007. **103**(6): p. 3865-3870.
31. Megelski, S., et al., *Micro-and nanostructured surface morphology on electrospun polymer fibers*. Macromolecules, 2002. **35**(22): p. 8456-8466.
32. Xin, Y. and D.H. Reneker, *Hierarchical polystyrene patterns produced by electrospinning*. Polymer, 2012. **53**(19): p. 4254-4261.
33. Li, D. and Y. Xia, *Direct fabrication of composite and ceramic hollow nanofibers by electrospinning*. Nano letters, 2004. **4**(5): p. 933-938.
34. Zhao, Y., X. Cao, and L. Jiang, *Bio-mimic multichannel microtubes by a facile method*. Journal of the American Chemical Society, 2007. **129**(4): p. 764-765.
35. Chen, H., et al., *Nanowire-in-Microtube Structured Core/Shell Fibers via Multifluidic Coaxial Electrospinning*. Langmuir, 2010. **26**(13): p. 11291-11296.
36. Jiang, Z., et al., *Magnetic PVF/Fe₃O₄@ PS Mat via Electrospinning for Oil Clean-up*.
37. Ko, H., et al., *Flexible Carbon - Nanofiber Connectors with Anisotropic Adhesion Properties*. Small, 2010. **6**(1): p. 22-26.
38. Li, W.J., et al., *Electrospun nanofibrous structure: a novel scaffold for tissue engineering*. Journal of biomedical materials research, 2002. **60**(4): p. 613-621.
39. Yoshimoto, H., et al., *A biodegradable nanofiber scaffold by electrospinning and its potential for bone tissue engineering*. Biomaterials, 2003. **24**(12): p. 2077-2082.

40. Sill, T.J. and H.A. von Recum, *Electrospinning: applications in drug delivery and tissue engineering*. Biomaterials, 2008. **29**(13): p. 1989-2006.
41. Kenawy, E.-R., et al., *Release of tetracycline hydrochloride from electrospun poly (ethylene-co-vinylacetate), poly (lactic acid), and a blend*. Journal of controlled release, 2002. **81**(1): p. 57-64.
42. Lee, S. and S.K. Obendorf, *Use of electrospun nanofiber web for protective textile materials as barriers to liquid penetration*. Textile Research Journal, 2007. **77**(9): p. 696-702.
43. Kang, Y.K., et al., *Application of electrospun polyurethane web to breathable waterproof fabrics*. Fibers and Polymers, 2007. **8**(5): p. 564-570.
44. Kim, I.-D., et al., *Microsphere templating as means of enhancing surface activity and gas sensitivity of $\text{CaCu}_3\text{Ti}_4\text{O}_{12}$ thin films*. Nano letters, 2006. **6**(2): p. 193-198.
45. Xiang, Q., et al., *Ag nanoparticle embedded-ZnO nanorods synthesized via a photochemical method and its gas-sensing properties*. Sensors and Actuators B: Chemical, 2010. **143**(2): p. 635-640.
46. Chae, H.G., et al., *Carbon nanotube reinforced small diameter polyacrylonitrile based carbon fiber*. Composites Science and Technology, 2009. **69**(3-4): p. 406-413.
47. Ren, L., R. Ozisik, and S.P. Kotha, *Rapid and Efficient Fabrication of Multilevel Structured Silica Micro-/Nanofibers by Centrifugal Jet Spinning*. Journal of Colloid and Interface Science, 2014(0).
48. Sarkar, K., et al., *Electrospinning to Forcespinning™*. Materials Today, 2010. **13**(11): p. 12-14.

49. R. T. Weitz, L.H., S. Rauschenbach, M. Burghard, K. Kern, *Polymer Nanofibers via Nozzle-Free Centrifugal Spinning*. Nano Lett, 2008. **8**(4): p. 1187-1191.
50. Badrossamay, M.R., et al., *Nanofiber assembly by rotary jet-spinning*. Nano Lett, 2010. **10**(6): p. 2257-2261.
51. Lu, Y., et al., *Parameter study and characterization for polyacrylonitrile nanofibers fabricated via centrifugal spinning process*. European Polymer Journal, 2013. **49**(12): p. 3834-3845.
52. Padron, S., *2D modeling of Forcespinning (TM) nanofiber formation with experimental study and validation*. 2012, The University Of Texas-Pan American.
53. Ramakrishna, S., *An introduction to electrospinning and nanofibers*. 2005: World Scientific.
54. Mo, X., et al., *Electrospun P (LLA-CL) nanofiber: a biomimetic extracellular matrix for smooth muscle cell and endothelial cell proliferation*. Biomaterials, 2004. **25**(10): p. 1883-1890.
55. Magarvey, R. and L. Outhouse, *Note on the break-up of a charged liquid jet*. Journal of fluid mechanics, 1962. **13**(01): p. 151-157.
56. Du, J. and X. Zhang, *Role of polymer-salt-solvent interactions in the electrospinning of polyacrylonitrile/iron acetylacetonate*. Journal of Applied Polymer Science, 2008. **109**(5): p. 2935-2941.
57. Shanmuganathan, K., et al., *Solventless high throughput manufacturing of poly (butylene terephthalate) nanofibers*. ACS Macro Letters, 2012. **1**(8): p. 960-964.

58. Wang, L., et al., *Fabrication of polymer fiber scaffolds by centrifugal spinning for cell culture studies*. *Microelectronic Engineering*, 2011. **88**(8): p. 1718-1721.
59. Ren, L., et al., *Large-scale and highly efficient synthesis of micro- and nano-fibers with controlled fiber morphology by centrifugal jet spinning for tissue regeneration*. *Nanoscale*, 2013. **5**(6): p. 2337-45.
60. Ren, L., et al., *Template Free and Large-Scale Fabrication of Silica Nanotubes with Centrifugal Jet Spinning*. *Chemical Engineering Journal*, 2014.
61. Baicheng Weng, F.X., Karen Lozano, *Mass Production of Carbon Nanotube-Reinforced Polyacrylonitrile Fine Composite Fibers*. *Journal of Applied Polymer Science*, 2014(40302).
62. Baicheng Weng, F.X., Alfonso Salinas and Karen Lozano, *Mass Production of Carbon Nanotube reinforced Poly(methyl methacrylate) Nonwoven Nanofiber Mats*. *Carbon*, 2014.
63. Weng, B., et al., *The production of carbon nanotube reinforced poly(vinyl) butyral nanofibers by the Forcespinning® method*. *Polymer Engineering & Science*, 2014: p. n/a-n/a.
64. Altecór, A., et al., *Mixed-valent VOx/polymer nanohybrid fibers for flexible energy storage materials*. *Ceramics International*, 2014. **40**(3): p. 5073-5077.
65. Ji, L., et al., *Recent developments in nanostructured anode materials for rechargeable lithium-ion batteries*. *Energy & Environmental Science*, 2011. **4**(8): p. 2682.
66. Zhang, X., et al., *Electrospun Nanofiber-Based Anodes, Cathodes, and Separators for Advanced Lithium-Ion Batteries*. *Polymer Reviews*, 2011. **51**(3): p. 239-264.

67. Liu, N., et al., *A yolk-shell design for stabilized and scalable li-ion battery alloy anodes*. Nano Lett, 2012. **12**(6): p. 3315-21.
68. Guo, Z., et al., *TiO₂(B) nanofiber bundles as a high performance anode for a Li-ion battery*. RSC Advances, 2013. **3**(10): p. 3352.
69. Qie, L., et al., *Nitrogen-doped porous carbon nanofiber webs as anodes for lithium ion batteries with a superhigh capacity and rate capability*. Advanced Materials 2012. **24**(15): p. 2047-50.
70. Zhou, X.-y., et al., *Silicon@carbon hollow core-shell heterostructures novel anode materials for lithium ion batteries*. Electrochimica Acta, 2013. **87**: p. 663-668.
71. Al, Q.e., *Graphene Networks Anchored with Sn@Graphene as Lithium Ion Battery Anode*. ACS Nano, 2014.
72. Wu, H., et al., *Engineering empty space between Si nanoparticles for lithium-ion battery anodes*. Nano Lett, 2012. **12**(2): p. 904-9.
73. Ji, L. and X. Zhang, *Electrospun carbon nanofibers containing silicon particles as an energy-storage medium*. Carbon, 2009. **47**(14): p. 3219-3226.
74. Yuan, S., et al., *Engraving Copper Foil to Give Large - Scale Binder - Free Porous CuO Arrays for a High - Performance Sodium - Ion Battery Anode*. Advanced Materials, 2014.
75. Lu, Y., et al., *Preparation and characterization of carbon-coated NaVPO₄F as cathode material for rechargeable sodium-ion batteries*. Journal of Power Sources, 2014. **247**: p. 770-777.

76. Slater, M.D., et al., *Sodium - Ion Batteries*. Advanced Functional Materials, 2013. **23**(8): p. 947-958.
77. Qian, J., et al., *High capacity and rate capability of amorphous phosphorus for sodium ion batteries*. Angewandte Chemie, 2013. **125**(17): p. 4731-4734.
78. Zhang, S.S., *Liquid electrolyte lithium/sulfur battery: fundamental chemistry, problems, and solutions*. Journal of Power Sources, 2013. **231**: p. 153-162.
79. Yang, Z., et al., *In situ synthesis of lithium sulfide-carbon composites as cathode materials for rechargeable lithium batteries*. Journal of Materials Chemistry A, 2013. **1**(4): p. 1433.
80. Ahn, W., et al., *Synthesis and electrochemical properties of a sulfur-multi walled carbon nanotubes composite as a cathode material for lithium sulfur batteries*. Journal of Power Sources, 2012. **202**: p. 394-399.
81. Jung, H.G., et al., *An improved high-performance lithium-air battery*. Nat Chem, 2012. **4**(7): p. 579-85.
82. Ryu, H., et al., *Discharge reaction mechanism of room-temperature sodium-sulfur battery with tetra ethylene glycol dimethyl ether liquid electrolyte*. Journal of Power Sources, 2011. **196**(11): p. 5186-5190.
83. Tarascon, J.-M. and M. Armand, *Issues and challenges facing rechargeable lithium batteries*. Nature, 2001. **414**(6861): p. 359-367.
84. Goodenough, J.B., H. Abruna, and M. Buchanan, *Basic research needs for electrical energy storage*. Report of the basic energy sciences workshop for electrical energy storage, 2007. **186**.

85. Yuan, X., H. Liu, and J. Zhang, *Lithium-ion batteries: advanced materials and technologies*. 2011: CRC Press.
86. Mukherjee, R., et al., *Nanostructured electrodes for high-power lithium ion batteries*. *Nano Energy*, 2012. **1**(4): p. 518-533.
87. Thackeray, M.M., W.I.F. David, and J.B. Goodenough, *Structural characterization of the lithiated iron oxides $Li_xFe_3O_4$ and $Li_xFe_2O_3$* . *Materials Research Bulletin*, 1982. **17**(6): p. 785-793.
88. Padhi, A.K., K. Nanjundaswamy, and J.B.d. Goodenough, *Phospho - olivines as positive - electrode materials for rechargeable lithium batteries*. *Journal of the Electrochemical Society*, 1997. **144**(4): p. 1188-1194.
89. Allen, M.J., V.C. Tung, and R.B. Kaner, *Honeycomb carbon: a review of graphene*. *Chemical reviews*, 2009. **110**(1): p. 132-145.
90. Chen, P., L. Guo, and Y. Wang, *Graphene wrapped SnCo nanoparticles for high-capacity lithium ion storage*. *Journal of Power Sources*, 2013. **222**: p. 526-532.
91. Zou, Y. and Y. Wang, *NiO nanosheets grown on graphene nanosheets as superior anode materials for Li-ion batteries*. *Nanoscale*, 2011. **3**(6): p. 2615-2620.
92. de las Casas, C. and W. Li, *A review of application of carbon nanotubes for lithium ion battery anode material*. *Journal of Power Sources*, 2012. **208**(0): p. 74-85.
93. Yazami, R., *Nanomaterials for Lithium-Ion Batteries: Fundamentals and Applications*. 2013: CRC Press.
94. Ando, Y., et al., *Physical properties of multiwalled carbon nanotubes*. *International journal of inorganic materials*, 1999. **1**(1): p. 77-82.

95. Thess, A., et al., *Crystalline ropes of metallic carbon nanotubes*. Science-AAAS-Weekly Paper Edition, 1996. **273**(5274): p. 483-487.
96. Lahiri, I., et al., *High capacity and excellent stability of lithium ion battery anode using interface-controlled binder-free multiwall carbon nanotubes grown on copper*. ACS nano, 2010. **4**(6): p. 3440-3446.
97. Landi, B.J., et al., *Carbon nanotubes for lithium ion batteries*. Energy & Environmental Science, 2009. **2**(6): p. 638-654.
98. Ng, S.H., et al., *Single wall carbon nanotube paper as anode for lithium-ion battery*. Electrochimica Acta, 2005. **51**(1): p. 23-28.
99. Chen, W.X., J.Y. Lee, and Z. Liu, *Electrochemical lithiation and de-lithiation of carbon nanotube-Sn₂Sb nanocomposites*. Electrochemistry communications, 2002. **4**(3): p. 260-265.
100. Mordkovich, V., *Carbon nanofibers: a new ultrahigh-strength material for chemical technology*. Theoretical Foundations of Chemical Engineering, 2003. **37**(5): p. 429-438.
101. Merkulov, V.I., et al., *Alignment mechanism of carbon nanofibers produced by plasma-enhanced chemical-vapor deposition*. Applied Physics Letters, 2001. **79**(18): p. 2970-2972.
102. Merkulov, V.I., et al., *Patterned growth of individual and multiple vertically aligned carbon nanofibers*. Applied Physics Letters, 2000. **76**(24): p. 3555-3557.
103. Rodriguez, N.M., *A review of catalytically grown carbon nanofibers*. Journal of Materials Research, 1993. **8**(12): p. 3233-3250.

104. Fitzer, E., W. Frohs, and M. Heine, *Optimization of stabilization and carbonization treatment of PAN fibres and structural characterization of the resulting carbon fibres*. Carbon, 1986. **24**(4): p. 387-395.
105. Ji, L., et al., *Preparation and characterization of silica nanoparticulate-polyacrylonitrile composite and porous nanofibers*. Nanotechnology, 2008. **19**(8): p. 085605.
106. Zhou, D.-D., et al., *A nitrogen-doped ordered mesoporous carbon nanofiber array for supercapacitors*. Journal of Materials Chemistry A, 2013. **1**(29): p. 8488.
107. Chou, S.-L., et al., *Enhanced reversible lithium storage in a nanosize silicon/graphene composite*. Electrochemistry Communications, 2010. **12**(2): p. 303-306.
108. Magasinski, A., et al., *High-performance lithium-ion anodes using a hierarchical bottom-up approach*. Nat Mater, 2010. **9**(4): p. 353-8.
109. Xiang, H., et al., *Graphene/nanosized silicon composites for lithium battery anodes with improved cycling stability*. Carbon, 2011. **49**(5): p. 1787-1796.
110. Xue, L., et al., *Si/C composite nanofibers with stable electric conductive network for use as durable lithium-ion battery anode*. Nano Energy, 2013. **2**(3): p. 361-367.
111. Li, S., et al., *Nanosized Ge@CNF, Ge@C@CNF and Ge@CNF@C composites via CVD method for use in advanced lithium-ion batteries*. Journal of Power Sources, 2013.
112. Howe, J.Y., et al., *Improving microstructure of silicon/carbon nanofiber composites as a Li battery anode*. Journal of Power Sources, 2013. **221**: p. 455-461.

113. Klankowski, S.A., et al., *A high-performance lithium-ion battery anode based on the core-shell heterostructure of silicon-coated vertically aligned carbon nanofibers*. *Journal of Materials Chemistry A*, 2013. **1**(4): p. 1055.
114. Wang, B., et al., *Contact-engineered and void-involved silicon/carbon nanohybrids as lithium-ion-battery anodes*. *Adv Mater*, 2013. **25**(26): p. 3560-5.
115. Zhang, W.-M., et al., *Tin-Nanoparticles Encapsulated in Elastic Hollow Carbon Spheres for High-Performance Anode Material in Lithium-Ion Batteries*. *Advanced Materials*, 2008. **20**(6): p. 1160-1165.
116. Yan Lu, L.G., Changbao Zhu, Joachim Maier, *Tin Nanoparticles Encapsulated in Porous Multichannel Carbon Microtubes:Preparation by Single-Nozzle Electrospinning and Application as Anode Material for High-Performance Li-Based Batteries*. *JACS Communications*, 2009. **131**: p. 15984–15985.
117. Yu, Y., et al., *Encapsulation of Sn@carbon nanoparticles in bamboo-like hollow carbon nanofibers as an anode material in lithium-based batteries*. *Angew Chem Int Ed Engl*, 2009. **48**(35): p. 6485-9.
118. Zou, L., et al., *Sn/C non-woven film prepared by electrospinning as anode materials for lithium ion batteries*. *Journal of Power Sources*, 2010. **195**(4): p. 1216-1220.
119. Zou, L., et al., *A film of porous carbon nanofibers that contain Sn/SnOx nanoparticles in the pores and its electrochemical performance as an anode material for lithium ion batteries*. *Carbon*, 2011. **49**(1): p. 89-95.
120. Fu, K., et al., *Effect of CVD carbon coatings on Si@CNF composite as anode for lithium-ion batteries*. *Nano Energy*, 2013. **2**(5): p. 976-986.

121. Zhang, L.Q., et al., *Direct observation of Sn crystal growth during the lithiation and delithiation processes of SnO₂ nanowires*. *Micron*, 2012. **43**(11): p. 1127-1133.
122. Osiak, M., et al., *Structuring Materials for Lithium-ion Batteries: Advancements in Nanomaterial Structure, Composition, and Defined Assembly on Cell Performance*. *Journal of Materials Chemistry A*, 2014.
123. Yoo, H.D., et al., *On the challenge of developing advanced technologies for electrochemical energy storage and conversion*. *Materials Today*, 2014. **17**(3): p. 110-121.
124. Su, D.S. and R. Schlogl, *Nanostructured carbon and carbon nanocomposites for electrochemical energy storage applications*. *ChemSusChem*, 2010. **3**(2): p. 136-68.
125. Miller, J.R. and P. Simon, *Electrochemical capacitors for energy management*. *Science Magazine*, 2008. **321**(5889): p. 651-652.
126. Li, X. and B. Wei, *Supercapacitors based on nanostructured carbon*. *Nano Energy*, 2013. **2**(2): p. 159-173.
127. Simon, P., Y. Gogotsi, and B. Dunn, *Where Do Batteries End and Supercapacitors Begin?* *Science*, 2014. **343**(6176): p. 1210-1211.
128. Pandolfo, A. and A. Hollenkamp, *Carbon properties and their role in supercapacitors*. *Journal of power sources*, 2006. **157**(1): p. 11-27.
129. Conway, B.E., *Electrochemical supercapacitors*. 1999.
130. Eliad, L., et al., *Ion sieving effects in the electrical double layer of porous carbon electrodes: estimating effective ion size in electrolytic solutions*. *The Journal of Physical Chemistry B*, 2001. **105**(29): p. 6880-6887.

131. Ghosh, A. and Y.H. Lee, *Carbon-Based Electrochemical Capacitors*. ChemSusChem, 2012. **5**(3): p. 480-499.
132. Gamby, J., et al., *Studies and characterisations of various activated carbons used for carbon/carbon supercapacitors*. Journal of Power Sources, 2001. **101**(1): p. 109-116.
133. Futaba, D.N., et al., *Shape-engineerable and highly densely packed single-walled carbon nanotubes and their application as super-capacitor electrodes*. Nature materials, 2006. **5**(12): p. 987-994.
134. Pröbstle, H., M. Wiener, and J. Fricke, *Carbon aerogels for electrochemical double layer capacitors*. Journal of Porous Materials, 2003. **10**(4): p. 213-222.
135. Vivekchand, S., et al., *Graphene-based electrochemical supercapacitors*. Journal of Chemical Sciences, 2008. **120**(1): p. 9-13.
136. Liu, C., et al., *Graphene-based supercapacitor with an ultrahigh energy density*. Nano letters, 2010. **10**(12): p. 4863-4868.
137. Kim, B.-H., K.S. Yang, and J.P. Ferraris, *Highly conductive, mesoporous carbon nanofiber web as electrode material for high-performance supercapacitors*. Electrochimica Acta, 2012. **75**: p. 325-331.
138. Merino, C., et al., *Carbon nanofibres and activated carbon nanofibres as electrodes in supercapacitors*. Carbon, 2005. **43**(3): p. 551-557.
139. Chen, Z., et al., *High-Performance Supercapacitors Based on Intertwined CNT/V2O5 Nanowire Nanocomposites*. Advanced Materials, 2011. **23**(6): p. 791-795.

140. Hong, J.-i., I.-H. Yeo, and W.-k. Paik, *Conducting Polymer with Metal Oxide for Electrochemical Capacitor: Poly (3, 4-ethylenedioxythiophene) RuO_x Electrode*. Journal of The Electrochemical Society, 2001. **148**(2): p. A156-A163.
141. Yang, L., et al., *Hierarchical network architectures of carbon fiber paper supported cobalt oxide nanonet for high-capacity pseudocapacitors*. Nano letters, 2011. **12**(1): p. 321-325.
142. Ra, E.J., et al., *High power supercapacitors using polyacrylonitrile-based carbon nanofiber paper*. Carbon, 2009. **47**(13): p. 2984-2992.
143. Wang, H., et al., *The effect of tin content to the morphology of Sn/carbon nanofiber and the electrochemical performance as anode material for lithium batteries*. Electrochimica Acta, 2011. **58**: p. 44-51.
144. Chen, J., et al., *Ultrasmall Sn nanoparticles embedded in nitrogen-doped porous carbon as high-performance anode for lithium-ion batteries*. Nano Lett, 2013.
145. Yu, Y., et al., *Reticular Sn nanoparticle-dispersed PAN-based carbon nanofibers for anode material in rechargeable lithium-ion batteries*. Electrochemistry Communications, 2010. **12**(9): p. 1187-1190.
146. Teo, W., et al., *Porous tubular structures with controlled fibre orientation using a modified electrospinning method*. Nanotechnology, 2005. **16**(6): p. 918.
147. Alamein, M.A., et al., *Nanospiderwebs: Artificial 3D Extracellular Matrix from Nanofibers by Novel Clinical Grade Electrospinning for Stem Cell Delivery*. Advanced Healthcare Materials, 2013. **2**(5): p. 702-717.

148. Theron, S.A., et al., *Multiple jets in electrospinning: experiment and modeling*. Polymer, 2005. **46**(9): p. 2889-2899.
149. Yang, Y., et al., *A shield ring enhanced equilateral hexagon distributed multi-needle electrospinning spinneret*. Dielectrics and Electrical Insulation, IEEE Transactions on, 2010. **17**(5): p. 1592-1601.
150. Jacob, M. and A. Arof, *FTIR studies of DMF plasticized polyvinylidene fluoride based polymer electrolytes*. Electrochimica acta, 2000. **45**(10): p. 1701-1706.
151. Phadke, M.A., et al., *Poly (acrylonitrile) ultrafiltration membranes. I. Polymer - salt - solvent interactions*. Journal of Polymer Science Part B: Polymer Physics, 2005. **43**(15): p. 2061-2073.
152. Padhye, M.R. and A.V. Karandikar, *The effect of alkali salt on solvent-polyacrylonitrile interaction*. Journal of Applied Polymer Science, 1985. **30**(2): p. 667-673.
153. Mahalingam, S. and M. Edirisinghe, *Forming of polymer nanofibers by a pressurised gyration process*. Macromol Rapid Commun, 2013. **34**(14): p. 1134-9.
154. Wang, Y., H.C. Zeng, and J.Y. Lee, *Highly reversible lithium storage in porous SnO₂ nanotubes with coaxially grown carbon nanotube overlayers*. Advanced Materials, 2006. **18**(5): p. 645-649.
155. Simon, P. and Y. Gogotsi, *Materials for electrochemical capacitors*. Nature materials, 2008. **7**(11): p. 845-854.
156. Frackowiak, E. and F. Beguin, *Carbon materials for the electrochemical storage of energy in capacitors*. Carbon, 2001. **39**(6): p. 937-950.

157. Jung, K.-H., et al., *Carbon nanofiber electrodes for supercapacitors derived from new precursor polymer: Poly(acrylonitrile-co-vinylimidazole)*. *Electrochemistry Communications*, 2012. **23**: p. 149-152.
158. Kim, C. and K.S. Yang, *Electrochemical properties of carbon nanofiber web as an electrode for supercapacitor prepared by electrospinning*. *Applied Physics Letters*, 2003. **83**(6): p. 1216.
159. Kim, C., *Electrochemical characterization of electrospun activated carbon nanofibres as an electrode in supercapacitors*. *Journal of Power Sources*, 2005. **142**(1-2): p. 382-388.
160. Ma, C., et al., *Phenolic-based carbon nanofiber webs prepared by electrospinning for supercapacitors*. *Materials Letters*, 2012. **76**: p. 211-214.
161. Seo, M.-K. and S.-J. Park, *Electrochemical characteristics of activated carbon nanofiber electrodes for supercapacitors*. *Materials Science and Engineering: B*, 2009. **164**(2): p. 106-111.
162. McDonough, J.R., et al., *Carbon nanofiber supercapacitors with large areal capacitances*. *Applied Physics Letters*, 2009. **95**(24): p. 243109.
163. Gao, Y., et al., *Chemical vapor-deposited carbon nanofibers on carbon fabric for supercapacitor electrode applications*. *Nanoscale research letters*, 2012. **7**(1): p. 1-8.
164. V. Barranco, M.A.L.-R., A. Linares-Solano, A. Oya, F. Pico, J. Iban, F. Agullo-Rueda, J. M. Amarilla, J. M. Rojo, *Amorphous Carbon Nanofibers and Their Activated Carbon Nanofibers as Supercapacitor Electrodes*. *J. Phys. Chem. C* 2010.

165. Kim, C., et al., *Self - Sustained Thin Webs Consisting of Porous Carbon Nanofibers for Supercapacitors via the Electrospinning of Polyacrylonitrile Solutions Containing Zinc Chloride*. *Advanced Materials*, 2007. **19**(17): p. 2341-2346.
166. Frackowiak, E., et al., *Supercapacitors based on conducting polymers/nanotubes composites*. *Journal of Power Sources*, 2006. **153**(2): p. 413-418.
167. Chen, L.-F., et al., *Synthesis of nitrogen-doped porous carbon nanofibers as an efficient electrode material for supercapacitors*. *ACS nano*, 2012. **6**(8): p. 7092-7102.
168. Li, L., et al., *Effect of compounding process on the structure and electrochemical properties of ordered mesoporous carbon/polyaniline composites as electrodes for supercapacitors*. *Journal of Power Sources*, 2009. **187**(1): p. 268-274.